

Medical imaging diagnosis of early Alzheimer's disease

Fatma El-Zahraa A. El-Gamal^{1,2}, Mohammed M. Elmogy^{1,2}, Mohammed Ghazal^{2,3}, Ahmed Atwan¹, Manuel F. Casanova⁴, Gregory N. Barnes⁵, Ayman S. El-Baz^{2*}, Hassan Hajjiab³

¹Information Technology Department, Faculty of Computers and Information, Mansoura University, 35516, Mansoura, Egypt, ²BioImaging Laboratory, Department of Bioengineering, University of Louisville, 40292, ³Department of Electrical and Computer Engineering, Abu Dhabi University, UAE, ⁴School of Medicine, University of South Carolina, 29208, Greenville, South Carolina, USA, ⁵University of Louisville Autism Center, Department of Neurology, University of Louisville, 40217, Louisville, KY, USA

TABLE OF CONTENTS

1. Abstract
2. Introduction
 - 2.1. Pre-AD stage
 - 2.2. Early (mild) AD
 - 2.3. Intermediate (moderate) AD
 - 2.4. Late (Severe) AD
3. Imaging in AD
 - 3.1. Magnetic resonance imaging (MRI)
 - 3.2. Emission-computed tomography (ECT)
 - 3.2.1. PET related studies
 - 3.2.2. Single photon emission computed tomography (SPECT)
 - 3.3. Other modalities
 - 3.3.1. Functional magnetic resonance imaging (fMRI)
 - 3.3.2. Diffusion tensor imaging (DTI)
 - 3.4. Fusion related studies
4. Challenges and future trends
 - 4.1. Databases
 - 4.2. Modalities
 - 4.3. Applied techniques
 - 4.4. Subjects
5. Conclusion
6. Acknowledgements
7. References

1. ABSTRACT

Alzheimer's disease (AD) is one of the most common neurodegenerative diseases that influences the central nervous system, often leading to dire consequences for quality of life. The disease goes through some stages mainly divided into early, moderate, and severe. Among them, the early stage is the most important as medical intervention has the potential to alter the natural progression of the condition. In practice, the early diagnosis is a challenge since the neurodegenerative changes can precede the onset of clinical symptoms by 10–15 years. This factor along

with other known and unknown ones, hinder the ability for the early diagnosis and treatment of AD. Numerous research efforts have been proposed to address the complex characteristics of AD exploiting various tests including brain imaging that is massively utilized due to its powerful features. This paper aims to highlight our present knowledge on the clinical and computer-based attempts at early diagnosis of AD. We concluded that the door is still open for further research especially with the rapid advances in scanning and computer-based technologies.

2. INTRODUCTION

Alzheimer's disease (AD) is a neurodegenerative disease that affects the central nervous system (CNS), causing dementia as described by the World Health Organization (1). Statistically, AD is the most common neurodegenerative disease among the elderly population, accounting for approximately 70 % of all cases of dementia (2). The incidence of AD increases with age, affecting 6 % of people between 70 and 74 years and reaching a prevalence of 42% in individuals over 85 years old. Although less common, early-onset forms of AD can occur in people younger than 70 years of age (3).

The seriousness of AD is manifested in the progressive nature of the condition. The AD patient presents with worsening clinical features including progressive cognitive deficits and disturbances of thought, perception, affect, and behaviors. The patient's cerebrum is afflicted with neurofibrillary tangles, neuritic plaques, neuronal loss, Hirano bodies, granulovacuolar degeneration, and amyloid angiopathy, all pathologies present in differing degrees from one patient to another (4). The progressive neurological decline, with the consequent loss of memory and the ability to perform basic daily activities, may prove fatal (5).

As is the case with many diseases, the early diagnosis of AD can help to preserve patients' quality of life, with therapies aimed at slowing the progression of the disease (6). However, the early diagnosis of AD is a challenging task due in part to the diversity of clinical features that can manifest in the disease's earliest stages (4). Moreover, the onset of neuropathological features characteristic of AD may precede the onset of clinical symptoms by ten to fifteen years. The delay may allow for massive neurodegeneration to occur undetected. Finally, the ambiguity about the pathophysiology of the disease and any putative cause(s) add to the challenges for an early diagnosis of AD.

There have been many scientific endeavors to clarify this complex disease. These efforts have looked at common features found in AD patients' medical history, mental and the physical status, laboratory tests, neurological, neuropsychological, and psychiatric evaluations, as well as neuroimaging findings (7). Of these tests, there has been the extensive utilization of brain imaging due to its increasing clinical availability and utility. Neuroimaging modalities have the ability to rule out other structural abnormalities as well as evaluate both the location and the degree of atrophy. Some modalities play a role in assessing metabolic abnormalities when the structural abnormalities are either absent or inconclusive. Finally, brain imaging can identify preclinical and mild cognitive impairment

(MCI) in AD, which facilitates the implementation of possible innovative therapeutic endeavors (8). It is important to note that brain scans are still expected to provide much more diagnostic and clinical utility, especially with the rapid development of new scanning technologies and analysis tools.

Before discussing the studies of the imaging technologies related to AD, a little background on the neuropathology of AD can provide a better understanding of the disease, as well as clarify the challenges faced by patients who struggle with this progressive disorder.

2.1 Neuropathology of AD

AD is one of the two most common degenerative diseases of the CNS, the other being Parkinson's disease. AD is characterized by two types of lesion commonly used to diagnose the disease a posteriori: extracellular neuritic plaques (previously called senile plaques) and neurofibrillary tangles (10). Extracellular neuritic plaques form in the neuropil surrounding the neurons and interfere with their functionality (11, 12). Within the neurons themselves, the abnormal structures known as neurofibrillary tangles build up, suppress the intracellular transport system, and finally cause cell death. The ensuing cellular loss leads to memory deficits and, as the process continues, brain shrinkage that results in gradual loss of function (11, 12).

Various areas of the brain are differentially affected throughout the course of the disease. Neurodegenerative changes are first manifested in the hippocampal formation and the entorhinal cortex, impacting the ability to form memories. From there it progresses to other areas of the temporal lobe, influencing hearing which can lead to suspicion and misunderstanding because of communication problems. Parietal lobes are the next brain region to be affected, with a consequent loss of ability to integrate visual, auditory, and somatosensory information. The frontal lobes are last to be affected, leading to socially inappropriate/unacceptable behavior and impaired judgment and reasoning.

2.2. Staging of AD progression

Systems have been devised to classify the degree to which AD has progressed. There are three such systems, known as three-, six- and seven-stage classification strategies. Among these classifications, the three-stage and seven-stage strategies are the most commonly used (13), with the latter being a refinement of the former. Of the two, the three-stage strategy is more widely used. Therefore, a brief description of the three-stage strategy and the main characteristics of each stage is presented while more

details regarding the seven-stage strategy can be found through Ali (13):

1. Pre-AD: In this stage, the disease-related symptoms are common even with persons not afflicted with AD. Therefore, any abnormality in daily life activities will not be noticed at a level which would cause concern.
2. Early (mild) AD: At this point, the abnormalities begin to be obvious, leading the patient to be concerned about his/her memory and get frustrated or angry. They do not correctly accomplish job assignments and have difficulties in performing tasks in a social setting
3. Intermediate (moderate) AD: The disease spreads and covers a larger area of the brain that influences sensory processing, reasoning, and thoughts. The patients' forgetfulness now includes old facts, which contributes to difficulties in performing required duties and increases the rate of agitation.
4. Late (severe) AD: It is the last and most difficult stage that faces the AD patients' family and caregivers due to the expansion of the damaged nerve cells making the patient require around-the-clock assistance. The patient will have difficulty walking, making him or her susceptible to complications such as pneumonia.

3. IMAGING IN AD

Medical imaging technologies have an effective role in revealing how the pathology of AD influences the brain. For instance, magnetic resonance imaging (MRI) technology can define the common occurrence of atrophy of the temporal lobes' medial structures (i.e., hippocampus and entorhinal cortex) in AD patients (14). Diffusion tensor imaging (DTI) measures the fiber tract integrity that directly helps in assessing the fibers of the white matter (WM). In addition, it reflects any disruption in the axons through the random movement of water molecules in tissues. Therefore, DTI facilitates the characterization of AD since such disruption would cause a reduction in the anisotropy (i.e., the water molecules' movement along the neural tract length is greater than those across the tract's width). Also, the regional analysis of the DTI shows that the changes in the hippocampal microstructure may represent a better indicator of the MCI progression risk to AD (15).

Studying both the resting and the activation states of the functional magnetic resonance imaging (fMRI) technology indicates the lesser-coordinated activity of AD patients compared with normal subjects in the hippocampus, inferior parietal lobes, and the cingulate cortex. Single photon emission computed tomography (SPECT), and positron emission tomography (PET), the main applications of emission-computed tomography (ECT) medical imaging modalities, reflect the detail of the progression of

brain changes (14). PET technology is considered a powerful tool for demonstrating the alterations of brain function by reflecting the brain condition at a molecular and cellular level. Before reviewing the current role of the other technologies in the early diagnosis of AD, a description of the AD stages will be presented.

As previously mentioned, the early diagnosis of AD can assist in prolonging and enhancing the AD patient's life. Despite the constant attempts of researchers to enhance knowledge in this area, the early diagnosis of the disease remains a challenge. Various scientific efforts were proposed throughout the last few decades to address the significant role of brain imaging in the early diagnosis of AD. These studies delineated the progression of AD and removed the ambiguity that surrounds the disease.

There is some reviews in the recent literature, summarizing the current advances regarding the early detection of AD (16–27). Some of these reviews focus only on specific brain imaging modalities, while others consider the combination of neuroimaging with other AD-related biomarkers. These reviews highlight findings in the preclinical or the MCI stage of AD. The present review, while also describing anatomical and clinical findings regarding stage 1 and stage 2 AD, primarily deals with computer-based methods that assist in defining these stages. Focus on the methodology is due to the rapid advances in biomedical imaging, which are leading to powerful new tools in diverse areas computer-assisted medicine including the management of AD. The review is organized by the significance of the modalities as follows: structural MRI is described first, followed by ECT modalities, and lastly the lesser used modalities, fMRI and DTI. After presenting the studies in each of these modalities, we discuss fusion methods where multi-modal data are combined to provide more informative results that consequently assist the early diagnosis of AD.

3.1. Magnetic resonance imaging (MRI)

MRI is a widely used, powerful assistive technology in diagnosing a variety of pathologies. This role is due to the level of detail and contrast it can achieve in its tomographic reconstructions. Besides differentiating tissue types by chemical composition (hydrogen content), MRI can additionally determine viscosity, stiffness, and protein content of the tissues (14). With signal intensity dependent on proton density and magnetization (spin-spin and spin-lattice relaxation times, T1 and T2, respectively), MRI is capable of unparalleled soft tissue definition for a non-invasive procedure (28, 29).

In AD, MRI has been widely utilized to study brain atrophy, which commonly occurs first in medial structures of the temporal lobe (21–32). Some studies

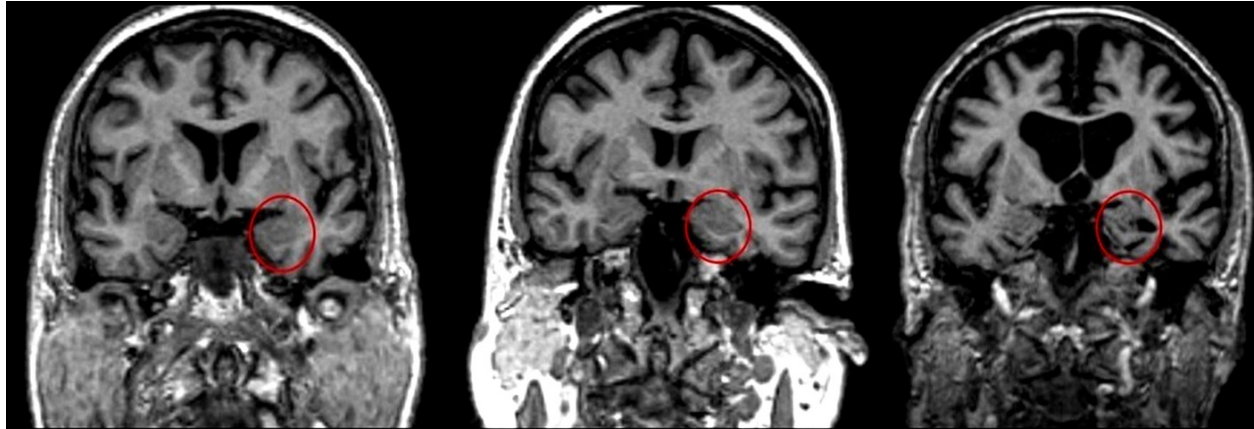


Figure 1. Examples of MRI-based visualization of three subjects: NC, MCI, and AD (left to right). The red circles show the degree of hippocampus atrophy that absents in NC, start to appear in MCI and clearly appeared in the AD subject.

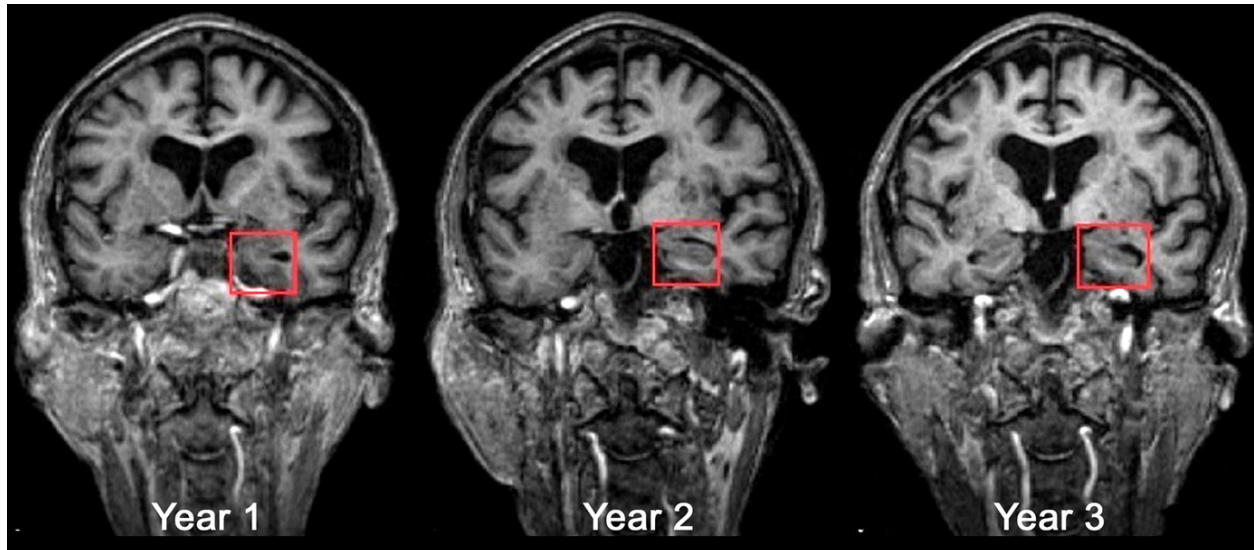


Figure 2. Different scans show the progression of the brain atrophies in an MCI subject with a year separating between each scan and the next. The red rectangles show the progression of the atrophies in the entorhinal cortex, hippocampus, amygdala and parahippocampus.

have demonstrated the progression of atrophy from entorhinal cortex to the hippocampus, amygdala, and parahippocampus (33–36). Additionally, the analysis of MRI has demonstrated the association between atrophy in MCI patients and the increased risk of developing AD that in turn helps in predicting future decline in healthy adults' memory. Besides such investigations, the volumetric analysis of the structural MR imaging technique may assist in detecting significant changes in the volumes of different brain regions, which in turn represent a promising indicator for the diagnosis process during the progression of AD (26). Examples of MRI-based visualization of the brain atrophy in an MCI subject and throughout the disease progression are presented in Figure 1 and Figure 2, respectively.

Yang *et al.* (37) introduced a classification framework of AD, amnesic MCI (aMCI), and dysexecutive MCI (dMCI). Further details regarding the difference between aMCI and dMCI can be found through Pa *et al.* (38). This framework used principal component analysis (PCA) for feature reduction and a self-organizing map (SOM) for the classification task. In addition, the study evaluated the accuracy of using volume features, shape features, a combination of the two, and both of them in addition to PCA-derived features. The results showed superior classifier performance when combining volume, shape and PCA. Although there was an improvement in the classification results, weak results were obtained all cases differentiating aMCI from dMCI.

Wolz *et al.* (39) aimed to examine four MRI related features in AD: hippocampal volume (HV), tensor-based morphometry (TBM), cortical thickness (CTH), and a feature extracted from a recently proposed manifold-based learning (MBL) through performing a classification task. For classification, support vector machine (SVM) and linear discriminant analysis (LDA) with these features were tested. The evaluation of utilizing the features individually showed that TBM provided the best results followed by MBL. Evaluating the classifiers showed that LDA obtained the best results on individual features. Finally, the combination of all features provided the most stable and reliable results of classification.

Varghese *et al.* (40) proposed a computer-aided diagnosis (CAD) system built on the combination of the bacterial foraging optimization (BFO) along with artificial neural network (ANN) to assist in the early diagnosis of AD. The proposed method illustrated that BFO-ANN segmentation algorithm could be used to distinguish between normal and abnormal MRIs of the brain. The method achieved classification accuracy up to 92%.

Mahmood and Ghimire (41) presented an automated system for diagnosing AD. This study was characterized by two aspects. First, rather than reducing the dimensionality of image descriptors to three dimensions as in the related work, which could compromise the information and consequently reduce the accuracy, they applied PCA to reduce it to 150 dimensions. The goal of this procedure was to preserve as much information as possible while still reducing dimensionality. Second, a multi-stage, multi-class feed forward ANN was adopted to help in classifying AD into its different stages starting from AD to Severe AD. The system achieved nearly 90% correct classification.

Shi *et al.* (42) focused on the automatic segmentation of the hippocampal subfields due to their relation to the early pathology of AD. Therefore, they introduced an automatic segmentation method that showed competitive results compared with related methods. Additionally, they proposed an exponential function-based, label fusion strategy for fitting the normalized case of the similarity measure and reported on the effectiveness of such a strategy when tested.

Mondal *et al.* (43) generated a brain atlas, which was represented by invariant feature key-points computed from a specific population. The entire brain was considered as a whole for such generation. Application of this atlas to the automated detection of AD-related changes showed major advantages of the whole-brain approach over localized methods. The results also showed that the proposed system has a satisfactory performance regarding early diagnosis of AD with sensitivity and a mean specificity of 97%

and 88%, respectively. For the diagnosis of AD, while excluding the very mild class, the system obtained sensitivity and mean specificity of 73% and 76%, respectively.

Nayaki and Varghese (31) focused on identifying MCI patients using a variety of greyscale texture operators to extract features from the gray matter (GM). The texture operators used by these authors were local binary pattern (LBP), local ternary pattern (LTP), dominant local binary pattern (DLBP), complete local binary pattern (CLBP), adaptive local binary pattern (ALBP), local quinary pattern (LQP), local graph structure (LGS), and a custom variant of LBP. They found that classification by LQP showed the highest accuracy, at 81%, followed by LGS-based classification with 80%.

López-Rodríguez and García-Linares (44) targeted the early diagnosis of AD through proposing image processing methodology, population model, and automatic system. The proposed image processing methodology aimed to ensure the results' related statistical validity. The population model targeted the structural changes noted in the progression of the disease from the initial stages of mild cognitive deterioration until the most advanced form. Regarding results, the proposed early diagnosis system reported classification results that exceed 90% accuracy. Also, testing GM related volumetric parameters of the NC versus AD subjects showed that the highest volumetric differences take place in the early stages of AD.

Payan and Montana (45) introduced a prediction method of AD-related stages through utilizing sparse autoencoders and convolutional neural networks (CNN). The novelty of the study included the usage of 3D convolution kernels on the MRI volume as a whole rather than 2D convolution kernels on the slices. They compared results of 2D and 3D convolution for different classification scenarios, including binary classifications (AD vs. NC, AD vs. MCI, and NC vs. MCI) and 3-way classification (AD, MCI or NC). Comparing the convolutions in such scenarios showed, in most cases, the more accurate results of the 3D convolution over 2D.

Khedher *et al.* (46) proposed a CAD system to assist in the early diagnosis of AD. The study tested the performance of two feature extractors, PCA and partial least squares (PLS), and also two SVM classifiers, linear SVM and SVM with the radial basis function (RBF) kernel. In general, the study found that PLS provided better classification in less computational time than PCA. Also, linear SVM provided good classification results, while more samples or smaller feature vectors were needed to make RBF provide good results. In the same context, Khedher *et al.* (47) combined independent component analysis (ICA)

along with SVM classifier to produce a CAD system, the goal of which was to assist in the early diagnosis of AD. To perform that, the segmented WM and GM were tested individually and after combining them. The findings support the combination of both results due to its impact in improving the classification accuracy.

Eskildsen *et al.* (30) proposed an automatic prediction system through focusing mainly on five key features: the left and right hippocampi gradings and the left precuneus' CTH, left superior temporal sulcus, in addition to right anterior parahippocampal gyrus. The predictive value of the system achieved 72%, which reflected the significance of these features to be utilized for the early diagnosis of AD.

Salvatore *et al.* (32) worked on revealing sensitive and specific MR related markers that in turn assisted in the early diagnosis of AD through a machine learning approach. The study found that the cerebellum was not implicated in AD-related atrophy. Also, the pathological changes in the temporal cortex, hippocampus, entorhinal cortex, thalamus, insular cortex, anterior cingulate cortex, orbitofrontal cortex, and precuneus, assist in discriminating MCI patients who later converted to AD (MCI-C) from those who did not (MCI-NC), when those patients were clinically and cognitively matched.

Hosseini-Asl *et al.* (48, 49) utilized deep learning to introduce a classification/prediction framework that served in the early diagnosis of AD. There are three key components regarding the proposed framework. First, the framework was capable of performing domain adaptation through detecting and extracting AD biomarker related characteristics from one domain (called the source), while performing the classification in another domain (called the target). Regarding the feature extraction, the framework could extract discriminative features that captured the anatomical variations (i.e., CTH and volume, brain size, ventricle size, and hippocampus model) through pre-training the 3D convolutional auto-encoder (3D CAE). Finally, the classification task was performed through stacking the trained 3D CAE with a fine-tuning to accomplish the required task through 3D-CNN. As compared to other state-of-the-art models, the proposed framework showed better classification results, which in turn serve in the early diagnosis of AD.

Liu *et al.* (50) focused on assisting the classification task of AD/MCI using an inherent structure-based multi-view learning (ISML) method. The proposed method went through multiple processes. These processes started with nonlinear registration for each MRI onto multiple selected templates. The goal of this step was to obtain multi-view feature representation from different templates

for each subject. Then, a feature selection procedure was performed based on a sub-class clustering process. After that, multiple SVM classifiers were utilized followed by fusion of these SVMs through an ensemble classification method with a simple majority voting strategy. In general, the proposed method showed better results than related state-of-the-art methods.

Maicas *et al.* (51) focused on the hippocampi to determine the most damaged regions through a spectral shape analysis method. The method relied on three different shape descriptors at each vertex of a triangulated mesh representation of the segmented hippocampus: heat kernel signature (HKS), the scale-invariant HKS (SIHKS), and the wave kernel signature (WKS). The authors' spectral segmentation method aimed to find which zones encode more identification information of AD within these descriptors. In brief, the results showed that SIHKS was the best descriptor in detecting AD from zone 3. Further details regarding the study and its results can be found in Table 2. Tables 1–5 present the details regarding the MRI studies arranged based upon the studied brain region.

3.2. Emission-computed tomography (ECT)

ECT is a medical imaging modality that deals with physiology rather than anatomy as in structural imaging modalities. The main subtypes of ECT are SPECT and PET. The difference between the two is that in SPECT technology, radioisotopes are employed that in turn decay is emitting a single gamma photon, while in PET technology, isotopes are employed in each annihilation where a couple of photons are produced (52).

SPECT assists in the differential diagnosis of dementia. In addition, it serves as an accurate tool for measuring the progression of the disease (26). Regarding AD, SPECT has identified changes in the anterior medial temporal lobes, posterior cingulate, and posterior temporoparietal cortex (53–56) as shown in Figure 3. PET has proven a powerful tool for demonstrating the alterations of the brain functions, in healthy controls or dementia patients, with imaging reflecting properties of the brain at the molecular and cellular level. In AD, PET technology has led to very accurate diagnostic algorithms. PET is used to differentiate between AD and other dementia disorders. Although SPECT is cheaper than PET, SPECT is less specific in its findings. Finally, it is important to note that combining SPECT and PET may help in both identifying as well as evaluating the early to late conditions of the patients (26).

There are mainly three classes of radiopharmaceuticals that have been recently used in functional imaging of the brain: markers of regional

Medical imaging diagnosis of early Alzheimer's disease

Table 1. The MRI studies based on structural characteristics

Ref.	41			
Approach details	Goal	CAD (BFO+ANN)		
	Notes	The Gabor filter was used for feature extraction.		
	Type	Supervised		
	Results	- The system achieved up to 92% accuracy. - It is possible to use the BFO ANN Segmentation algorithm for distinguishing between normal and abnormal MRIs of the brain.		
	Clinical findings	The accelerated loss in GM volume and other regions of the brain showed a discrimination between AD and NC.		
Dataset	Sree Chitra Tirunal institute for medical science and technology (SCTIMST)			
Scanning Char.	Siemens Magnetom-Avanto SQ engine, 1.5.T MR Scanner. Whole brain volume was acquired by the 3D flash spoiled gradient echo sequence using standard parameters. TR=11msec, TE=4.9.5, flip angle=150, slice thickness=1mm, matrix=256x256, 112 axial plane images were made to cover the whole brain.			
Brain Region	Structural characteristics			
Subjects	Group	NC	MCI	AD
	No.	20	30	-
	Age	52 to 75		-
System Char.	Automatic/Objective			
Ref.	42			
Approach details	Goal	Classification (multiclass neural network)		
	Notes	The PCA was used to reduce the dimensionality of the MR image vector to 150 dimensions due to the very high dimensionality of MRI scans.		
	Type	Supervised		
	Results	The proposed work achieved almost 90% of the classification accuracy.		
	Clinical findings	Providing a classification to different stages of AD.		
Dataset	Open access series of imaging studies (OASIS)			
Scanning Char.	-			
Brain Region	The structure of the brain.			
Subjects	Group	NC	MCI	AD
	No.	-	-	-
	Age	-	-	-
	Note:	- For training: 230 diagnosed MRIs provided by OASIS were used. - For testing: The whole OASIS dataset (457 MRIs) was used. - Regarding age: the adult life span in OASIS was aged 18 to 96.		
System Char.	Automatic/Objective			
Ref.	46			
Approach details	Goal	Classification (sparse autoencoders and CNN)		
	Notes	The main novelty of the proposed method was the use of 3D convolution on the whole MRI rather than 2D convolution on the slices.		
	Type	Supervised		
	Results	- The accuracy of the proposed method when using 2D and 3D convolutions for the purpose of binary classifications (AD vs. NC, AD vs. MCI and NC vs. MCI) and the purpose of 3-way classification (AD, MCI or NC) was evaluated. The results showed that: when comparing 2D and 3D convolutions, 3D convolution showed better results in all classification cases except for binary AD vs. NC where there is no noticeable difference between 2D and 3D convolutions.		
	Clinical findings	Assisting in predicting the patient status of the disease.		
Dataset	Alzheimer's disease neuroimaging association (ADNI)			
Scanning Char.	-			
Brain Region	Structure of the brain			
Subjects	Group	NC	MCI	AD
	No.	755	755	755
	Age	-	-	-
System Char.	Automatic/Objective			

Table 2. The MRI studies based on Hippocampus

Ref.	43			
Approach details	Goal	Segmentation (multi-atlas image segmentation with ELM based bias detection and correction technique)		
	Notes	<ul style="list-style-type: none"> - Symmetric mutual information energy was utilized to perform symmetric diffeomorphic registration in the Atlas. - Exponential label fusion strategy function was proposed for the case of normalized similarity measure in combining the segmentation. 		
	Type	Supervised		
	Results	<ul style="list-style-type: none"> - The proposed method showed effectiveness, especially for the larger hippocampal subfields with more than 80% of overlap. This provided competitive results compared with the related methods. - Also, the proposed label fusion strategy showed its effectiveness when tested. 		
	Clinical findings	- Improved the effectiveness of the automatic segmentation of the hippocampal subfields that in turn is related to the early diagnosis of AD.		
Dataset	Public brain atlas online			
Scanning Char.	Two types of images were used: MRI-T1 images with a resolution of $1.0 \times 1.0 \times 1.0 \text{ mm}^3$ MRI-T2 sagittal images with a resolution of $0.4 \times 0.5 \times 2 \text{ mm}^3$			
Brain Region	Hippocampal subfields			
Subjects	Group	NC	MCI	AD
	No.	-	-	-
	Age	-	-	-
	Note:	The dataset contained 32 samples and conducted ten experiment groups where each group is using ten different test samples.		
System Char.	Automatic/Objective			
Ref.	52			
Approach details	Goal	Automatic detection/Spectral shape analysis (merge spectral techniques based on the Laplace-Beltrami (LB) operator and a bag of features (BoF)).		
	Notes	<ul style="list-style-type: none"> - Three different shape descriptors at each vertex of the triangle mesh of segmented hippocampus were used, and these descriptors are HKS, the SIHKS and the WKS. - Each descriptor was used separately in a BOF framework that in turn was used for shape retrieval. - An anatomical structure segmentation that applies the neighborhood filter (NF) to decrease the rearrangement of the second eigenfunction of the LB operator was also proposed. This method was used to partition the hippocampus into three regions to explore whether one of them mostly encapsulates the early damages caused by this disorder. 		
	Type	-		
	Results	<ul style="list-style-type: none"> - For both used datasets: 1-Right hippocampus detection outperformed left hippocampus diagnosis in the maximum acceptance rates for all the descriptors. 2-SIHKS achieved the best performance when considering both hippocampi (left and right). 3-Combining the descriptors from both hippocampi in the case of SIHKS and HKS revealed more information. For WKS, it used right hippocampi for better distinguishing the normal from dementia patients. These results meant that better detection could be obtained through descriptors' combination and also revealed that the right hippocampus is more damaged by the disease. - Evaluating the proposed segmentation method that applied the NF and that partitions the hippocampi into three regions, showed that: 1-SIHKS encoded most of the information for detecting AD from zone 3 2-Region analysis using WKS as a signature described a similar behavior because encoding information from just region 2 was better than the general WKS approach by 1%. 3-No clear information was obtained by using HKS for local analysis. 4-The proposed technique benefited from image quality, and this was obvious due to the greater results obtained by 3T images of DEMCAM than 1.5 T images of ADNI. 		
	Clinical findings	The SIHKS was the most suitable descriptor for detecting AD.		
Dataset	DEMCAM and ADNI			
Scanning Char.	For DEMCAM: T1-weighted MR images acquired on a GE Healthcare Signa HDX 3Tscanner.			
Brain Region	Hippocampus			

Medical imaging diagnosis of early Alzheimer's disease

Subjects	Database	Group	NC	MCI	AD
	ADNI	No.	90	-	90
		Age	-	-	-
	DEMCAM	No.	19	-	19
		Age	-	-	-
System Char.	Automatic/Objective				

Table 3. The MRI studies based on GM

Ref.	32				
Approach details	Goal	Longitudinal analysis of GM changes in AD, MCI, and AD (Local patterns)			
	Notes	<ul style="list-style-type: none"> - Local patterns were used as a feature extraction mechanism - The used local patterns in the study were: LBP, LTP, DLBP, CLBP, ALBP, LQP, LGS and some variants of LBP. - SVM was used for the classification task 			
	Type	Supervised			
	Results	The study compared the local patterns and found that LQP showed the highest accuracy of 81% followed by LGS with 80%.			
	Clinical findings	MCI progresses faster than AD			
Dataset	ADNI				
Scanning Char.	T1-Weighted-3TMRI Scanner's using protocol-TR=3000, FOV=240*240mm ² , with 256*256*170 mm ³ -acquisition matrix in X Y Z dimensions-slice thickness 1.2mm, Siemens 3T MR Scanner-176 slices.				
Brain Region	Medial temporal lobe (MTL) where the GM was segmented from it.				
Subjects	Group	NC	MCI	AD	
	No.	125	125	125	
	Age	65.3	69.3	64.9	
System Char.	Automatic/Objective				
Ref.	45				
Approach details	Goal	Prediction (Artificial Intelligence and Data Mining (decision trees and MultiBoost technique))			
	Notes	<ul style="list-style-type: none"> - The study proposed a robust image processing model to ensure statistical validity of the results of neuroimaging studies. - The study developed a population model of the structural changes that occurred in the progression of the disease. 			
	Type	Supervised			
	Results	The classification of NC and AD subjects achieved accuracy exceeding 90%.			
	Clinical findings	The highest volumetric differences occur in the early disease-related stages; then the differences tend to cancel with age.			
Dataset	ADNI and OASIS				
Scanning Char.	-				
Brain Region	GM				
Subjects	Database	Group	NC	MCI	AD
	ADNI	No.	766	-	748
		Age	-	-	-
	OASIS	No.	421	-	165
		Age	-	-	-
System Char.	Automatic/Objective				

Medical imaging diagnosis of early Alzheimer's disease

Ref.	31				
Approach details	Goal	Prediction (Mutual information-based feature selection method + Linear discriminant classifier)			
	Notes	The mutual information-based feature selection method was utilized to optimize the classification of MCI converters through identifying five key features: left and right hippocampi gradings and CTHs of the left precuneus, left superior temporal sulcus, and right anterior part of the parahippocampal gyrus.			
	Type	Supervised			
	Results	The used features achieved a prediction accuracy of 72%.			
	Clinical findings	Assisting the experts in the early diagnosis of AD through revealing the significance of the extracted features.			
Dataset	ADNI				
Scanning Char.	-				
Brain Region	GM especially MTL structures and CTH <i>Note: the key features obtained using mutual information-based feature selection were the left and right hippocampi gradings and CTHs of the left precuneus, left superior temporal sulcus, and right anterior part of the parahippocampal gyrus.</i>				
Subjects	Group	NC	MCI		AD
	No.	231	MCI-C	MCI-NC	198
			167	238	
Age (mean±SD)	76.0±5.0	74.5±7.2	74.9±7.7	75.3±7.5	
System Char.	Automatic/Objective				
Ref.	51				
Approach details	Goal	Classification (ISML method+ ensemble classification method of multiple SVM with a simple majority voting strategy)			
	Notes	-			
	Type	Supervised			
	Results	Evaluating the accuracy reported 93.83%, 89.09% and 80.90% for classifying (AD vs. NC, MCI-C vs. NC, MCI-C vs. MCI-NC), respectively.			
	Clinical findings	Assisting the experts in the diagnosis of AD, including the early stages of the disease.			
Dataset	ADNI				
Scanning Char.	-				
Brain Region	GM				
Subjects	Group	NC	MCI		AD
	No.	128	MCI-C	MCI-NC	97
			117	117	
Age	76.11±5.10	75.18±6.97	75.09±7.65	75.90±6.84	
System Char.	Automatic/Objective				

cerebral blood flow (rCBF), markers of regional cerebral metabolism, and CNS receptor binding agents (57). In any case, the patient is injected intravenously with the radiopharmaceuticals, then the SPECT or PET scanner is used to measure the regional uptake and distribution of the radiotracers. Measurement of rCBF relies on lipophilic radiopharmaceutical agents that are diffused from the arterial vascular compartment to the normal compartment of the brain tissue. The tracers are proportionally distributed to the blood flow of the regional tissue with an irreversible trapping in the tissue compartment. Measurement of regional cerebral metabolism is performed through transporting the applied radiopharmaceuticals through

regional cerebral blood flow to the brain tissues. Subsequently, the distribution of the regional cerebral reflects the utilization rate of the specific tracer in the cerebral metabolic pathway. Receptor binding agents measure the density as well as the binding affinity of the neuronal receptor through the use of suitable radiotracers (57). Table 6 shows the major agents from each class; reference (58) provides further details.

In addition to the tabulated radiotracers, Pittsburgh compound b (^{11}C -PiB) is a fluorescent analog of thioflavin T that helps in PET to visualize pathological hallmarks associated with AD. Therefore, it can be used in the investigation of the progression

Table 4. The MRI studies based on WM and GM

Ref.	47				
Approach details	Goal	CAD system (PLS or PCA+SVM with linear or (RBF) kernels)			
	Notes	- The study evaluates the performance of PCA and PLS as feature extraction methods. - Two SVM classifiers have been assessed with linear or RBF kernels			
	Type	Supervised			
	Results	<p>- Comparing WM, GM and WM+GM shows various results:</p> <p>1- The classification results of using only WM brain tissue provided better results than using only GM.</p> <p>2- The combination of GM and WM tissues in (NC vs. AD) and in (NC vs. MCI) showed better results than using these tissues individually. In the case of (MCI vs. AD), using WM was better than the combination which indicated that most important brain changes occur in WM than GM tissue.</p> <p>3- The classification results of (MCI vs. AD) reflected that the neurodegeneration effect of the disease starts in the WM and with the disease progression it spreads to the GM.</p> <p>- Evaluating the performance of the classification using PLS for feature extraction along with SVM classifier produced better classification and smaller computational time results than using PCA method.</p> <p>- The CAD system related performance improved with the number of the components of PLS and PCA used as input features to the classification that achieved a maximum stable value.</p> <p>- Linear SVM provided good results while more samples or smaller feature vectors were needed to obtain good results with RBF.</p> <p>- Regarding sensitivity, specificity, and accuracy, the proposed CAD system obtained maximize values of 85.11%, 91.27%, and 88.49%, respectively.</p>			
	Clinical findings	<p>- The important brain atrophy in the early study (MCI) occurs in WM rather than GM tissue.</p> <p>- The classification results of (MCI vs. AD) reflected that the neurodegeneration effect of the disease starts in the WM and with the disease progression it spreads to the GM.</p>			
Dataset	ADNI				
Scanning Char.	-				
Brain Region	GM and WM				
Subjects	Group	NC	MCI	AD	
	No.	229	401	188	
	Age (mean±SD)	75.97±5.0	74.85±7.4	75.36±7.5	
System Char.	Automatic/Objective				
Ref.	48				
Approach details	Goal	CAD system (ICA+SVM)			
	Notes	Two SVM classifiers were evaluated: with linear or RBF kernels			
	Type	Supervised			
	Results	<p>- Combining WM and GM tissues improved accuracy more than using these tissues individually.</p> <p>- The proposed method of combining ICA and SVM performed better than other related methods.</p>			
	Clinical findings	Assisting the experts in the early diagnosis of AD.			
Dataset	ADNI				
Scanning Char.	-				
Brain Region	WM and GM				
Subjects	Group	NC	MCI		AD
	No.	229	MCI-NC	MCI-C	188
			312	86	
	Age	-	-	-	-
System Char.	Automatic/Objective				

through the AD stages (26). In MCI and AD subjects, cerebral cortical retention of ¹¹C-PiB is present while most of the NC did not show that (59, 60). In MCI group, up to two-thirds of the studied patients showed levels of ¹¹C-PiB uptake and retention between that of NC and AD. This retention appears in the posterior

cingulate gyrus, anterior cingulate and frontal cortex (61, 62). Finally, the AD group presented a correlation between the retention and the anatomopathological distribution of dense β-amyloid plaques. The frontal cortex, cingulate gyrus, precuneus, and the striate, parietal, and lateral temporal cortexes showed the

Table 5. The MRI studies based on multiple brain regions

Ref.	38				
Approach details	Goal	Classification (SOM)			
	Notes	PCA was used for feature reduction.			
	Type	Supervised			
	Results	<ul style="list-style-type: none"> - Combining the volumetric and shape features improved the classification accuracy to 86.76%, 66.67% and 46.67% in AD, aMCI, and dMCI, respectively. - Testing the classification results using volume features, shape features, volume+shape features, and volume+shape+PCA features showed that the volume+shape+PCA features provided the best classification results with accuracies of 93.63%, 73.33% and 53.33% in AD, aMCI, and dMCI, respectively. - Despite the achieved accuracy, sensitivity and specificity in AD, aMCI, and dMCI, the classification results in aMCI and dMCI were not better than AD. This was due to similar characteristics between aMCI and AD, and dMCI and NC. 			
	Clinical findings	- Measuring global GM, WM and cerebrospinal fluid (CSF) volumes and the analysis of local shapes, especially in the ventricular area, perimeter properties, and distances properties, revealed atrophy related information.			
Dataset	Chang Gung Memorial Hospital, Lin-Kou, Taiwan				
Scanning Char.	The whole-brain MRI scans were obtained by a 3T MR scanner T1 MPRage series with TR = 2000ms and TE = 2.63ms. The results were represented as a 224×256 matrix, and slice thickness = 1mm in 160 slices.				
Brain Region	Volumetric and shape features				
Subjects	Group	NC	MCI		AD
	No.	28	aMCI	dMCI	24
			17	15	
Age	67 ± 5.67	70 ± 5.01	73 ± 5.13	71 ± 7.37	
System Char.	Automatic/Objective				
Ref.	40				
Approach details	Goal	Classification			
	Notes	<ul style="list-style-type: none"> - The study aimed to improve the accuracy of the classification through combining features revealed from different MRI analysis techniques. These features were HV, TBM, CTH and those extracted from a recently proposed MBL. - Two classifiers (LDA and SVM) were utilized, and their results were compared. 			
	Type	Supervised			
	Results	<ul style="list-style-type: none"> - Evaluating the utilized features individually showed that TBM was the best, closely followed by MBL while combining all the features improved the results. - Comparing SVM and LDA showed that LDA classifier achieved the best sensitivity and specificity results of 90%/84% (NC vs. AD), 64%/66% (MCI-NC vs. MCI-c) and 82%/76 (NC vs. MCI-C) with individual features. - The features combination improved the sensitivity and specificity results to 93%/85% (NC vs. AD), 67%/69%, (MCI-NC vs. MCI-C) and 86%/82% (NC vs. MCI-C). 			
	Clinical findings	<ul style="list-style-type: none"> - Among the evaluated features, TBM showed the best results, closely followed by MBL. - Combining the features improved the results. 			
Dataset	ADNI				
Scanning Char.	Standard 1.5.T screening/baseline T1-weighted images obtained using volumetric 3D MPRAGE protocol with resolutions ranging from 0.9. mm×0.9. mm×1.2.0 mm to 1.3. mm×1.3. mm×1.2.0 mm were included from the ADNI database.				
Brain Region	HV, TBM, CTH and features extracted from a recently proposed MBL.				
Subjects	Group	NC	MCI		AD
	No.	231	MCI-C	MCI-NC	198
			167	238	
Age	76.02	74.6	74.85	75.68	
System Char.	Automatic/Objective				

Medical imaging diagnosis of early Alzheimer's disease

Ref.	44			
Approach details	Goal	Brain atlas generation (invariant feature key-points' detection and description by 3D scale-invariant feature transform (SIFT))		
	Notes	<ul style="list-style-type: none"> - The model based MRI alignment technique was utilized, which helped in reducing search space for keypoint matching among different volumes. - A greedy approach has been introduced to obtain a set of invariant feature keypoints from multiple volumes of the brain. - The proposed method for brain atlas generation depended on the machine used for the acquisition of brain MR images, the spatial resolution used for the analysis, and the mode of imaging (i.e., T1 weighted, T2 weighted, etc.). - The proposed method considered the entire brain as a whole instead of considering mere individual organs. 		
	Type	-		
	Results	<p>- Evaluating the system showed the significant role of the very mild AD class in the early diagnosis. This appeared since:</p> <p>1-The experimental results showed a satisfactory performance of the proposed method for the application of an early diagnosis of AD with sensitivity and a mean specificity of 97% and 88%, respectively.</p> <p>2-For the diagnosis of AD, excluding the very mild class, the system obtained sensitivity and mean specificity of 73% and 76%, respectively.</p> <p>- Considering the entire brain volume for atlas generation represented a major advantage of the proposed technique</p>		
	Clinical findings	The system showed satisfactory performance regarding the early diagnosis of AD.		
Dataset	OASIS			
Scanning Char.	-			
Brain Region	The entire brain as a whole.			
Subjects	Group	NC	MCI	AD
	No.	30	-	-
	Age	33 to 70	-	-
	Note:	<ul style="list-style-type: none"> - For atlas generation: 30 NC brain volumes have been used. - For AD diagnosis, 165 brain volumes have been used for the experiments. 		
System Char.	Automatic/Objective			
Ref.	33			
Approach details	Goal	Classification (machine learning classifier proposed by (in paper) that is an optimization of SVM)		
	Notes	<ul style="list-style-type: none"> - The aim was to be able to extract spatially distributed multivariate diagnostic biomarkers from structural MR brain images to be used for both the early and accurate AD diagnosis. - The classifier went through two steps: <ul style="list-style-type: none"> 1-Feature extraction and selection (PCA+FDR). 2-Single-subject classification. 		
	Type	Supervised		
	Results	The accuracy results of (AD vs. NC), (MCI vs. NC) and (MCI-c vs. MCI-NC) were 76%, 72% and 66%, respectively (nested 20-fold cross validation).		
	Clinical findings	<ul style="list-style-type: none"> - The cerebellum was found to be not related to the AD-like atrophy. - Anatomical changes were detected in the posterior lobule of the cerebellum. - The AD-like atrophy patterns characterized by combined pathological changes within the temporal cortex, hippocampus, entorhinal cortex, thalamus, insular cortex, anterior cingulate cortex, orbitofrontal cortex, and precuneus allowed distinguishing clinically- and cognitively-matched MCI-C from MCI-NC. 		
Dataset	ADNI			
Scanning Char.	-			
Brain Region	Hippocampus, entorhinal cortex, basal ganglia, gyrus rectus, precuneus, and cerebellum were all critical regions known to be strongly involved in the pathophysiological mechanisms of AD.			
Subjects	Group	NC	MCI	AD
	No.	162	MCI-C 76	MCI-NC 134
	Age (range) (mean±SD)	(60–90) 76.3±5.4	(55–88) 74.8±7.4	(58–88) 74.5±7.2
				(55–91) 76.0±7.3
System Char.	Automatic/Objective			

Medical imaging diagnosis of early Alzheimer's disease

Ref.	49				
Approach details	Goal	Classification/Prediction (deep 3D-CNN)			
	Notes	<ul style="list-style-type: none"> - No skull-stripping was performed on the MRI data. - The proposed framework was capable of detecting and extracting AD biomarker related characteristic in the domain (called source) while performing the classification in another domain (called the target). 			
	Type	Supervised			
	Results	<ul style="list-style-type: none"> - The hierarchical feature extraction was improved in the hidden layer of the 3D-CNN. - The proposed framework showed better performance results compared with other state-of-the-art models. 			
	Clinical findings	Assisting the experts in the early diagnosis of AD.			
Dataset	30 subject from CAD Dementia (as a source domain) and 210 subjects from ADNI (as a target domain)				
Scanning Char.	-				
Brain Region	CTH and volume, brain size, ventricle size and hippocampus model				
Subjects	Database	Group	NC	MCI	AD
	subjects from ADNI	No.	70	70	70
		Age (mean ± SD)	75.0±7.9	75.9±7.7	74.6±6.1
System Char.	Automatic/Objective				
Ref.	50				
Approach details	Goal	Classification (3D-CAE+3D-CNN)			
	Notes	<ul style="list-style-type: none"> - 3D extension of CAE was used for unsupervised generic and transferable feature extraction of the source domain. - 3D-CNN was fine-tuned to perform classification task on the target domain. - For feature extraction through the pretrain 3D-CAE, the source domain data were preprocessed through spatial normalization then skull stripping and intensities normalization were performed. However, for the classification, the data were used without any preprocessing or skull stripping procedures. 			
	Type	Supervised			
	Results	The proposed system showed better accuracy results than related state-of-the-art models.			
	Clinical findings	Assisting the experts in the early diagnosis of AD.			
Dataset	CAD-Dementia (Source domain) and ADNI (target domain)				
Scanning Char.	-				
Brain Region	CTH and volume, brain size, ventricle size and hippocampus model				
Subjects	Database	Group	NC	MCI	AD
	ADNI	No.	70	70	70
		Age (mean±SD)	74.6±6.1	75.9±7.7	75.0±7.9
System Char.	Automatic/Objective				

greater regional binding. On the other hand, the occipital cortex, sensory and motor cortex, and mesial temporal cortex showed the lesser binding (63). To illustrate these findings, Figure 4 shows an example of ¹¹C-PiB PET scans of NC, MCI, and AD subjects. Also, Figure 5 shows ¹¹C-PiB scans of an MCI subject during different time periods.

¹⁸F-2-fluoro-2-deoxy-d-glucose (¹⁸F-FDG) is a marker of regional cerebral metabolism that measures the metabolism of glucose in different brain regions. This tracer can help to predict the conversion of MCI patients to AD, where patients who convert show hypometabolism in medial temporal and posterior cingulate cortices as compared to the NCs (64–66). The examination of FDG-PET shows severe

reductions of glucose consumption in the AD patients' brains compared to NC subjects. Figure 6 shows an example of different subjects' scans to illustrate the visualization of the disease's progression using FDG, while Figure 7 shows the alterations at different time periods of an MCI subject. Finally, usage of FDG and PiB tracers in PET scans indicates that the last tracer is more capable of early detection of the AD progression (26).

3.2.1. PET related studies

As previously mentioned, the PET scan is an accurate assistant for the diagnosis of AD. Numerous studies relied on this powerful technology to serve in decision-making at this early stage of the disease.

Table 6. The Major SPECT and PET radiotracers for the brain

	rCBF	Regional cerebral metabolism	CNS receptor binding agents
SPECT	<ul style="list-style-type: none"> - technetium-99m-hexamethylpropylene amine oxime (Tc-99m-HMPAO) - Tc-99m-ethyl cysteinatidimer (Tc-99m-ECD) - ... 	<ul style="list-style-type: none"> - In normal Brain: No tracers until now to measuring normal cerebral metabolism - In brain tumors: thallium-201 Tc-99m-methoxyisobutylnitrile (Tc-99m-MI-BI) 	I-123 q-CIT
PET	O-15 H ₂ O	<ul style="list-style-type: none"> - ¹⁸F-FDG - (F-18)-fluoro-3'-deoxy-3'-I-fluorothymidine (FLT) 	Hundreds of PET tracers

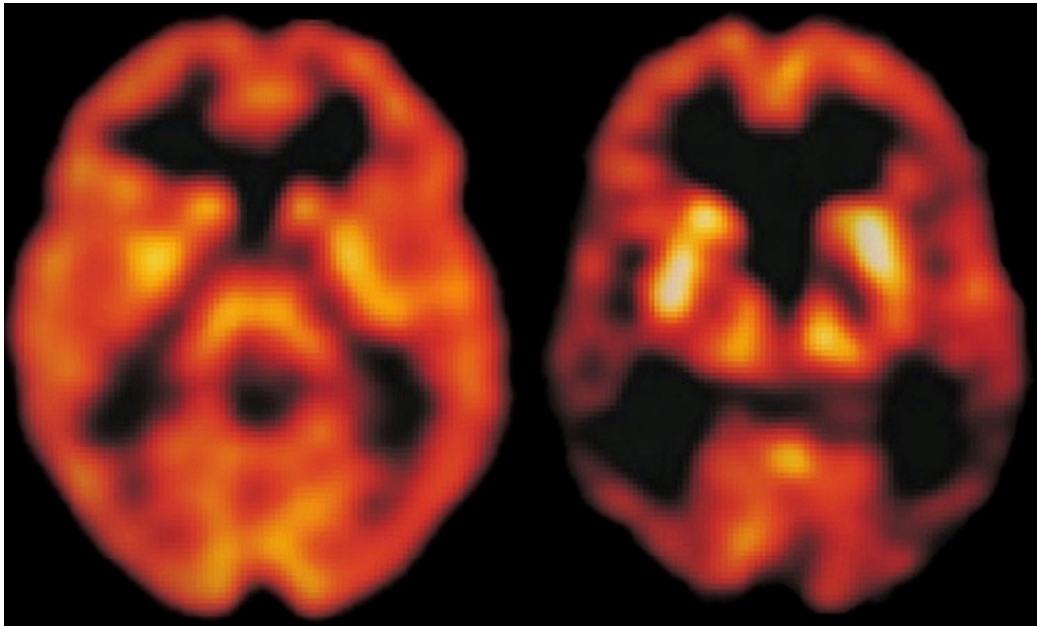


Figure 3. An example of 99mTc-HMPAO SPECT scan (50) (left) where the left is an NC scan within general uniform distribution of the tracer throughout the cortex along with slight “hyperperfusion” in the basal ganglia. On the other hand, the right is for AD patient with a general decrease in the perfusion throughout the cortex relatively with the cerebellum.

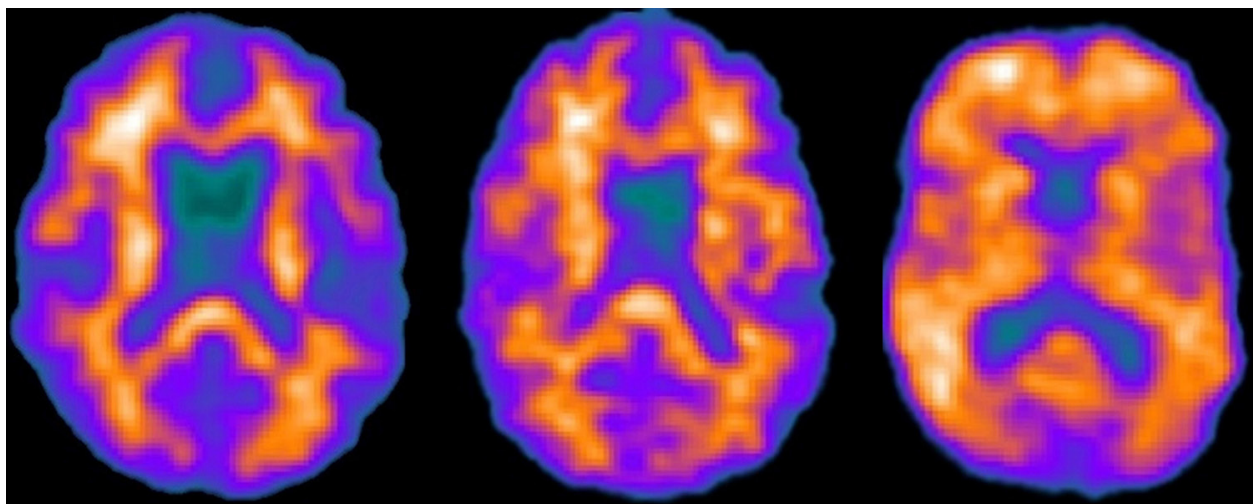


Figure 4. Examples of ¹¹C-PIB retention of three subjects NC, MCI, and AD, respectively from left to right where the brighter colors represent, the higher retention and vice versa.

Medical imaging diagnosis of early Alzheimer's disease

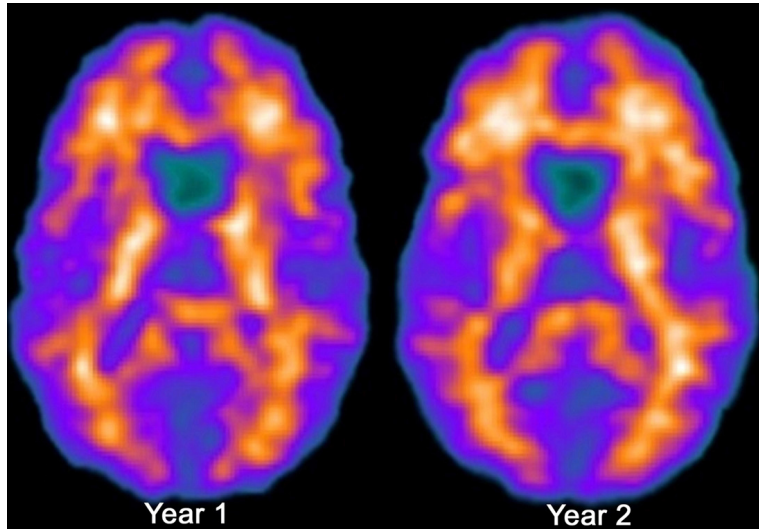


Figure 5. Different ^{11}C -PiB PET scans of an MCI subject that represent the progression of the disease through the increment of the retention illustrated through the brighter colors.

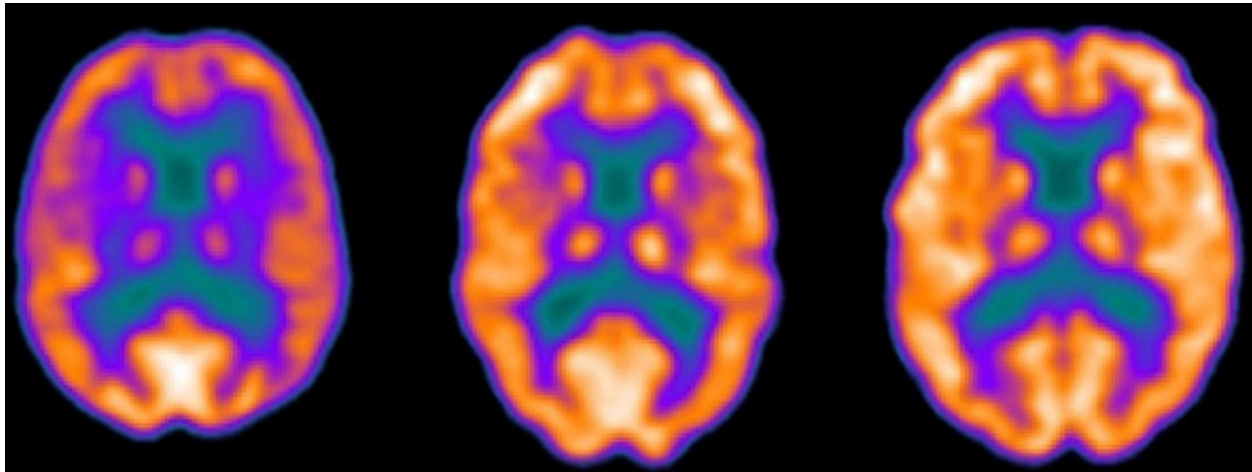


Figure 6. The variations on an MCI subject's scan on different time periods using ^{18}F -FDG that represent the hypometabolism between the two scans as the disease proceed.

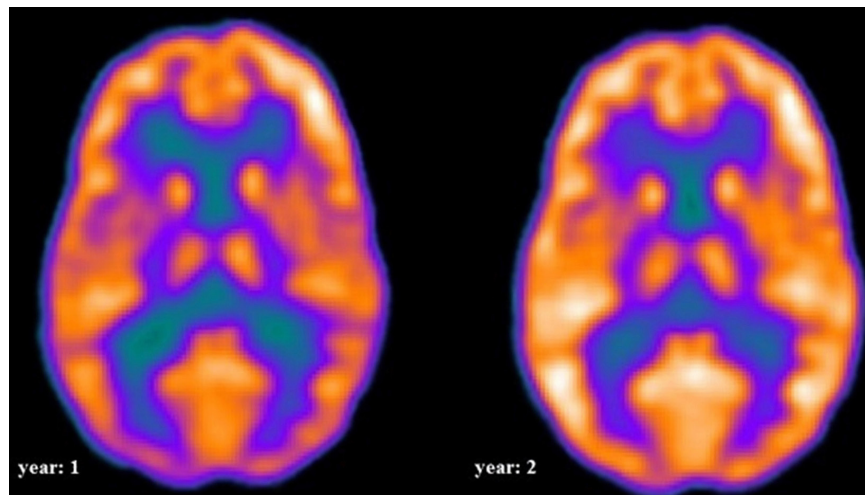


Figure 7. Examples of NC, MCI and AD subjects' ^{18}F -FDG scans that reveal the hypometabolism throughout the progression of the disease.

For example, Illán *et al.* (67) focused on comparing ^{18}F -FDG and PiB PET regarding the early diagnosis of AD. To accomplish such a comparison, the study applied an automatic classification system based on PCA and SVM. The results showed that ^{18}F -FDG and PiB had similar accuracy regarding AD diagnosis, while PiB was shown to have higher discriminative power than FDG in the case of very early AD. One year later, the same group (68) presented a CAD system that relied on an eigenimage framework for PET imaging that did not require an eigenbrain selection. The system encompassed several ideas, which were dimensionality reduction, feature extraction (with representative vector demixing using PCA/ICA), and classification. The results of the classification stage showed the accuracy of 88.24% in identifying AD.

López *et al.* (69) proposed a CAD system that relied on PCA along with LDA/Fisher discriminant ratio (FDR) to select the required features for the subsequent classification process that was carried out through ANN/SVM. The system was evaluated on two different databases of SPECT and PET images, with resulting accuracy up to 89.52% for PET scans.

Martínez-Murcia *et al.* (70) presented a CAD system that proceeding in three stages: voxel selection using Mann-Whitney-Wilcoxon U-Test, feature extraction using means of factor analysis, and classification based on linear SVM. The strength of the Mann-Whitney-Wilcoxon U-Test was in its resistance to outliers. The system was tested on two databases, one for SPECT and another for PET scans. Regarding PET, the system achieved an accuracy of 92.9% which in turn reflected the power of this system in serving the early diagnosis of AD.

Chaves *et al.* (71) relied on the association rule (AR) mining to construct a CAD system that served the early diagnosis of AD. The proposed system applied FDR and activation estimation (AE) for feature/region of interest (ROI) extraction. Then, AR was used for the classification task. FDR was used to reveal the selection of the most discriminant regions and to reduce computation cost. AE provided a trade-off between the computation complexities and the accuracy of the image classification, and it allowed all relevant brain regions to be included. The system performance was evaluated on two databases for PET and SPECT scans. Regarding PET, the classification accuracy of applying the system achieved 91.33%. Then, Chaves *et al.* (72) addressed the problem of the small sample size through combining ARs, PCA, and PLS to construct a CAD system that targeted the early stages of AD. This proposed combination produced a feature vector with a reduced dimension to overcome a smaller number of samples compared to the high dimension of the feature space. The proposed system was evaluated

on PET and SPECT scans. For PET scan, the system achieved an accuracy of 90%; that was better than other compared methods and thus assisted in the early diagnosis of the disease.

After that, Chaves *et al.* (15) aimed to provide early diagnosis of AD through integrating continuous attribute discretization (for the feature selection) along with the AR-mining (for classification). Before applying the discretization procedure, the histogram was calculated over a mean control image for the purpose of segmenting the image into subimages composed of voxels whose intensities belong to each bin. Therefore, this procedure could call image thresholding due to the separation of the objects based on their intensity level. The performance of the proposed system was evaluated on SPECT and PET databases. Using PET scans, the method attained 92% accuracy, improving on the authors' previous work on the early diagnosis of AD (71, 72).

Padilla *et al.* (73) proposed an NMF-SVM CAD system for early diagnosis of AD. This method employed nonnegative matrix factorization (NMF) and the FDR for the purpose of feature selection and SVM with bounds of confidence for the purpose of classification. To test the performance of the proposed system, two databases (PET and SPECT) were used where the system achieved up to 86 % of the classification accuracy of the PET data.

Toussaint *et al.* (74) targeted the early diagnosis of AD through a classification method (SVM) that relied on combining voxel-based group analysis and ICA. The purpose of such combination was to extract characteristic differential patterns from the PET scans. The results showed that the combination assisted in the discrimination task and the accuracy of classification achieved 80%.

Morbelli *et al.* (75) focused on analyzing the voxel-wise interregional correlation by means of a statistical parametric mapping to reveal information that consequently serves the early diagnosis of AD. The results, in general, showed that the AD pathophysiological process seems to be associated with large-scale of functional brain network alterations. Default mode network (DMN) and networks that support memory function are particularly involved in this alterations.

Ayhan *et al.* (76) focused on voxel-based analysis using composite kernels for a predictive model of AD. The Gaussian process (GP) was used for the predictive modeling. The results showed that the composite kernels helped to reveal the anatomical regions that were related to the disease. Additionally, comparing single and composite kernels either showed competitive or better results of the composite kernels.

Also, the composite kernels showed significantly improved discrimination between MCI and NC. A further goal of the study was to derive the automatic relevance determination down to the region level, thereby significantly reducing the computational requirements.

Aidos *et al.* (77) focused on comparing voxel regions extracted automatically against that extracted with the assistance of an expert. To accomplish that, three classifiers were used: SVM, k-nearest neighbors (KNN), and naïve Bayes classifiers. In general, the experiments showed best results with SVM and KNN when the automatic identification took place with better results of KNN compared with SVM.

Bilgel *et al.* (78) studied the temporal trajectories of amyloid deposition with the goal of better understanding their association with disease progression. Therefore, the study presented an estimation method of the temporal trajectories of voxelwise amyloid from the longitudinal PET images using expectation-maximization (EM) algorithm. The results of the study showed that the estimated longitudinal trajectory slopes revealed better localized longitudinal changes as compared with the age progression at each voxel. Much more details regarding the results of PET related studies are found in Table 7.

3.2.2. Single photon emission computed tomography (SPECT)

Many of the same labs working on PET have also studied the utility of SPECT in AD. For instance, Padilla *et al.* relied on the SPECT data in different studies (79–81). Their recent work (81) presented a CAD system capable of analyzing functional SPECT images to assist in the early diagnosis of AD. The system applied FDR to analyze the imaging data and NMF to select and extract discriminatory features, which were then used to train an SVM-based classifier. The findings showed classification accuracy up to 94%, thus improving on the PCA+SVM method. Regarding feature extraction, NMF showed better results when compared with PCA techniques. Finally, with regard to their CAD system (73) which combines NMF and SVM for feature selection/reduction and classification, respectively, the system achieved an accuracy up to 91% of SPECT data.

Ramírez *et al.* (82) constructed a CAD system that uses PCA/PLS regression model to perform feature extraction and random forest (RF) classifier to accomplish the classification task. Evaluating the system showed that a generalization error converged to a limit when the number of trees was increased in the forest. Therefore, the generalization error was reduced when using PLS and relied on the individual

forest trees' strength and the correlation between them. Finally, evaluating PCA and PLS on the data for extracting discriminative information showed that PLS was more efficient yielding peak accuracy values of 96.9%.

Salas-Gonzalez *et al.* (83) presented a CAD system to assist in the early diagnosis of AD. The system was composed of Welch's *t*-test for feature selection, and linear kernel based SVM/classification trees for classification tasks. Voxels were selected based on whether they are exceeding different threshold values after applying Welch's *t*-test. Then, the feature vectors were constructed through calculating mean and standard deviation (SD). The experimental results showed that classifying the subjects into normal and affected was performed in a parsimonious way without prior knowledge. Moreover, the system achieved the best classification accuracy (i.e., 96.2%) using classification trees, high sensitivity with SVM, and high specificity with decision trees.

Chaves *et al.* (84) presented a method for classification that aids with early diagnosis through applying the voxels-as-features (VAF) technique and AE in the feature extraction step while applying AR in the mining step. As a final step, the classification was carried out depending on some mined rules that were previously verified by each subject. Testing the results of two AR modes (supervised mode with the prior goal of 2 discriminant rules and unsupervised mode without any prior goals) showed the same accuracy, but better computation time with the supervised mode. Regarding classification accuracy results, the proposed method achieved an accuracy of 95.87% that represented a better result when compared with other reported methods.

Chaves *et al.* (85) subsequently proposed another classification method combining VAF, normalized minimum square error (NMSE), *t*-test selection, and kernel PCA (KPCA) in the feature extraction stage and kernel distance metric learning methods in the classification stage. The study compared three different metrics in the classification stage: Euclidean, Mahalanobis, energy-based distance. The results showed the highest classification accuracy of the energy-based method, achieving 96.91%. After that, they (72) proposed a CAD system that was based on AR-mining for feature selection, PCA/PLS for feature extraction and SVM for classification. They tested the system performance on SPECT and PET databases and achieved an accuracy of 91.75% with SPECT images. With the test on SPECT images of their proposed system (71) that was dependent on FDR and AE for feature/ROI extraction and AR for classification, the system achieved accuracy results of 92.78%. Finally, the classification accuracy achieved up to 96.91% for their system (15) that relied on

Table 7. The PET related studies for early diagnosis of AD

Ref.	68				
Approach details	Goal	Comparing the diagnostic accuracy of ¹⁸ F-FDG and PiB PET scans (Machine learning algorithm (PCA + SVM))			
	Notes	-			
	Type	Supervised			
	Results	While ¹⁸ F-FDG and PiB have similar diagnostic accuracy in AD, PiB was shown to have higher discriminative power in very early AD than FDG.			
	Clinical findings	Regarding the early diagnosis of AD, PiB was shown to have higher discriminative power than FDG.			
Dataset	¹⁸ F-FDG and PiB PET scans from ADNI				
Scanning Char.	-				
Brain Region	- Glucose metabolism (from ¹⁸ F-FDG PET) and amyloid deposition (from PiB PET).				
Subjects	Group	NC	MCI		AD
	No.	17	MCI-C	MCI-NC	19
			12	55	
	Age	76.5±4.8	75.1±7.4		77.2±7.2
System Char.	Automatic/Objective				
Ref.	69				
Approach details	Goal	CAD system (image projection (feature reduction) + eigenimage based decomposition (feature extraction) + SVM)			
	Notes	The PCA and ICA were evaluated to perform image projection for the purpose of feature reduction.			
	Type	Supervised			
	Results	The proposed system achieved 88.24% accuracy in AD identification.			
	Clinical findings	Assist in the early diagnosis of AD.			
Dataset	¹⁸ F-FDG PET from ADNI				
Scanning Char.	The PET data were acquired using Siemens, General Electric (GE), Philips, Siemens HRRT and BioGraph HiRez PET scanners. FDG PET scans were acquired according to a standardized protocol. A 30 min dynamic emission scan, consisting of 65 minframes, was acquired starting 30 min after the intravenous injection of 5.0 ± 0.5 mCi of ¹⁸ F-FDG, like the subjects, who were instructed to fast for at least 4 h prior to the scan, lay quietly in a dimly lit room with their eyes open and minimal sensory stimulation.				
Brain Region	Measuring the brain's rate of glucose metabolism with the ¹⁸ F-Fluorodeoxyglucose tracer.				
Subjects	Group	NC	MCI	AD	
	No.	97	209	95	
	Age	76.7 ± 5.2	76.0 ± 7.7	77.3 ± 7.4	
System Char.	Automatic/Objective				
Ref.	70				
Approach details	Goal	CAD system (PCA/LDA (feature extraction) + FDR (feature selection) +ANN/SVM (classification))			
	Notes	- The data were arranged into three different groupings to label the data into only two classes:			
		Grouping 1: All the data were considered where AD and MCI subjects were treated as positive and NC as negative.			
		Grouping 2: Only AD and NC subjects were considered, with AD treated as positive and NC as negative.			
	Grouping 3: Only MCI and NC subjects were considered, with MCI treated as positive and NC as negative.				
	Type	Supervised			
	Results	- The best combination of techniques that composed the complete CAD systems was not fixed but depends on the specific database and the classification task. However, in general, SVM provided better results than ANN with the same features.			
- When classes were best classified by linear surfaces or decision lines, the rearrangement of the PCA coefficients by the FDR criterion usually yielded higher accuracy rates.					
- FDR was useful when dealing with group 2, which was the best-described group regarding class separability using PCA+LDA features. However, it did not outperform PCA+LDA either for group 1 or group 3.					
- The system achieved a classification accuracy of 89.52%.					
Clinical findings	Assisting the experts in the early diagnosis of AD				
Dataset	¹⁸ F-FDG PET from ADNI				

Medical imaging diagnosis of early Alzheimer's disease

Scanning Char.	The data were acquired using Siemens, GE, and Philips PET scanners. PET data acquired from the Siemens HRRT and BioGraph HiRez scanners were excluded from the primary analysis due to differences in the pattern of FDG uptake.			
Brain Region	Measuring the rate of glucose metabolism with the tracer ^{18}F -Fluorodeoxyglucose			
Subjects	Group	NC	MCI	AD
	No.	52	114	53
	Age (mean \pm SD)	76.5 \pm 4.8	75.1 \pm 7.4	77.2 \pm 7.2
System Char.	Automatic/Objective			

Ref.	71			
Approach details	Goal	CAD system (voxel selection (Mann–Whitney–Wilcoxon U-Test), feature extraction (Factor Analysis) and classification (linear SVM))		
	Notes	<p>- Using Mann–Whitney–Wilcoxon selection criteria for the purpose of voxel selection represented one of the strengths of the proposed system due to its role in preventing the system from selecting outliers.</p> <p>- The purpose of proposing the factor analysis was to extract common factors and factor loadings from the selected voxels and thus helped in carrying out the feature reduction.</p>		
	Type	Supervised		
	Results	The classification accuracy achieves 92.9%.		
	Clinical findings	Assisting the experts in the early diagnosis of AD.		
Dataset	^{18}F -FDG PET from ADNI			
Scanning Char.	Baseline FDG-PET data acquired from Siemens, GE, Philips, Siemens HRRT and BioGraph HiRez PET scanner. FDG PET scans were acquired according to a standardized protocol. A 30 min dynamic emission scan, consisting of 65- min frames, was acquired starting 30 min after the intravenous injection of 5.0 ± 0.5 mCi of ^{18}F -FDG, like the subjects, who were instructed to fast for at least 4 h before the scan, lay quietly in a dimly lit room with their eyes open and minimal sensory stimulation.			
Brain Region	Measuring the brain's rate of glucose metabolism with the ^{18}F -Fluorodeoxyglucose tracer.			
Subjects	Group	NC	MCI	AD
	No.	The total number of participants was 401		
	Age	Enrolled subjects were between 55–90 (inclusive) years of age.		
System Char.	Automatic/Objective			

Ref.	72			
Approach details	Goal	CAD system (FDR and AE (feature/ROI extraction), AR (mining))		
	Notes	<p>- The FDR was used for enabling the selection of the discriminant regions for further analysis and for reducing the computational cost.</p> <p>- AE provided a trade-off between the computation complexities and the accuracy of the image classification in addition to allowing all relevant brain regions to be included.</p>		
	Type	Supervised		
	Results	The system achieved the accuracy of 91.33%		
	Clinical findings	Assisting the experts in the early diagnosis of AD.		
Dataset	^{18}F -FDG PET from ADNI			
Scanning Char.	FDG PET scans were acquired according to a standardized protocol. A 30-min dynamic emission scan, consisting of six 5-min frames, was acquired starting 30 min after the intravenous injection of 5.0 ± 0.5 mCi of ^{18}F -FDG, like the subjects, who were instructed to fast for at least 4 h prior to the scan, lay quietly in a dimly lit room with their eyes open and minimal sensory stimulation.			
Brain Region	Measures the rate of glucose metabolism with the tracer ^{18}F -Fluorodeoxyglucose			
Subjects	Group	NC	MCI	AD
	No.	75	-	75
	Age	-	-	-
System Char.	Automatic/Objective			

Medical imaging diagnosis of early Alzheimer's disease

Ref.	74				
Approach details	Goal	CAD system (analysis (FDR)+feature selection and extraction (NMF) + classification (SVM with bounds of confidence))			
	Notes	Three different approaches for the classifier were provided and detailed, two of them included bounds of confidence and took advantage of the definition of a "security region" in the SVM hyperplane, where no decision was assumed.			
	Type	Supervised			
	Results	The results achieved up to 86 % of the classification accuracy.			
	Clinical findings	Assisting the experts in the early diagnosis of AD.			
Dataset	¹⁸ F-FDG PET from ADNI				
Scanning Char.	-				
Brain Region	Measures the rate of glucose metabolism with the tracer ¹⁸ F-Fluorodeoxyglucose				
Subjects	Group	NC	MCI	AD	
	No.	52	114	53	
	Age	-	-	-	
System Char.	Automatic/Objective				
Ref.	75				
Approach details	Goal	Classification (univariate or multivariate statistical techniques + SVM)			
	Notes	The proposed method combined voxel-based group analysis and ICA for the purpose of extracting differential characteristic patterns from the PET scans.			
	Type	Supervised			
	Results	- Extracting visual or attentional components using spatial ICA could help in improving the discrimination accuracy. - Using the selected regions achieved an accuracy of 80%.			
	Clinical findings	- Improved the early detection and differentiation of typical vs. pathological metabolic patterns in the MCI subjects. - Early Identified in the development of the disease those individuals at high risk of rapid cognitive decline who could be candidates for new therapeutic approaches			
Dataset	ADNI				
Scanning Char.	-				
Brain Region	Cerebral glucose metabolism				
Subjects	Group	NC	MCI		prodromal AD (pAD)
	No.	80	MCI-C	MCI-NC	80
			40	40	
Age	76.4±4.6	76.4±4.1	76.4±4.2	76.0±6.3	
System Char.	Automatic/Objective				
Ref.	76				
Approach details	Goal	voxel-wise interregional correlation analysis (Statistical parametric mapping)			
	Notes	-			
	Type	-			
	Results and Clinical findings	- The area of hypometabolism in pAD showed less metabolic connectivity in patients than in NC (autocorrelation and correlation with large temporal and frontal areas, respectively). - pAD patients showed limited correlation even in selected nonhypometabolic areas, including the hippocampi and the dorsolateral prefrontal cortex (DLFC). - In NC group, the correlation was highlighted between hippocampi and precuneus/posterior cingulate and frontal cortex, and between DLFC and caudate nuclei and parietal cortex. - The reduced metabolic connections both in hypometabolic and nonhypometabolic areas in pAD patients suggested that metabolic disconnection (reflecting early diaschisis) may antedate remote hypometabolism (an early sign of synaptic degeneration).			
Dataset	¹⁸ F-FDG PET from European Alzheimer's disease consortium (EADC) project				
Scanning Char.	-				
Brain Region	Resting-state metabolic connectivity				
Subjects	Group	NC	aMCI	AD	
	No.	105	36	-	
	Age	68.7±6.4	72.1±8.4	-	
	Note: the aMCI is for amnesic MCI subjects who converted to AD after an average time of 2 years, pAD				
System Char.	Semiautomatic/Subjective				

Medical imaging diagnosis of early Alzheimer's disease

Ref.	73			
Approach details	Goal	CAD system (AR-mining and combination (feature selection) + PCA/PLS (feature extraction) + SVM (classification))		
	Notes	-		
	Type	Supervised		
	Results	The system achieved an accuracy of 90%.		
	Clinical findings	Assisting the experts in the early diagnosis of AD.		
Dataset	ADNI			
Scanning Char.	A 30-min dynamic emission scan, consisting of 6 5-min frames, was acquired starting 30 min after the intravenous injection of 5.0 ± 0.5 mCi of ^{18}F -FDG, like the subjects, who were instructed to fast for at least 4 h prior to the scan, lay quietly in a dimly lit room with their eyes open and minimal sensory stimulation.			
Brain Region	Measures the rate of glucose metabolism with the tracer ^{18}F -Fluorodeoxyglucose			
Subjects	Group	NC	MCI	AD
	No.	75	-	75
	Age (range) (mean \pm SD)	(62–86) (75.97 \pm 4.91)	-	(55–88) (75.72 \pm 7.40)
System Char.	Automatic/Objective			
Ref.	14			
Approach details	Goal	CAD system (continuous attribute discretization (feature selection) + AR mining (classification))		
	Notes	Image histogram segmentation was used over the mean control images to obtain the best mask that in turn was used in the feature selection step.		
	Type	Supervised		
	Results	Obtained a classification accuracy of 92%.		
	Clinical findings	Assisting the experts in the early diagnosis of AD		
Dataset	ADNI			
Scanning Char.	A 30-min dynamic emission scan, consisting of 6 5-min frames, was acquired starting 30 min after the intravenous injection of 5.0 ± 0.5 mCi of ^{18}F -FDG, as the subjects, who were instructed to fast for at least 4 h prior to the scan, lay quietly in a dimly lit room with their eyes open and minimal sensory stimulation.			
Brain Region	Measures the rate of glucose metabolism with the tracer ^{18}F -Fluorodeoxyglucose			
Subjects	Group	NC	MCI	AD
	No.	75	-	75
	Age (range) (mean \pm SD)	(62–86) (75.97 \pm 4.91)	-	(55–88) (75.72 \pm 7.40)
System Char.	Automatic/Objective			
Ref.	77			
Approach details	Goal	Voxel-based analysis (GPs by composite kernels)		
	Notes	<ul style="list-style-type: none"> - Two composite kernels were used: (SE and NN). - The aim of using composite kernel was to respond to the disease related characteristic patterns. 		
	Type	Supervised		
	Results	<ul style="list-style-type: none"> - The composite kernels helped to reveal the anatomical regions that are related to the disease. - Comparing single and composite kernels either showed competitive or better results of the composite kernels. - The composite kernels showed significant distinguishing improvement between MCI and NC. - Derived the automatic relevance determination toward the region level would significantly reduce the computation requirement. 		
	Clinical findings	Assist in the early diagnosis AD		
Dataset	ADNI			
Scanning Char.	-			
Brain Region	The metabolic activity of the cerebral cortex was used.			
Subjects	Group	NC	MCI	AD
	No.	101	230	60
	Age (mean)	76.1	75.6	77.4
System Char.	Automatic/Objective			

Medical imaging diagnosis of early Alzheimer's disease

Ref.	78			
Approach details	Goal	Comparing automatic and expert based identification of voxels regions for the discrimination task between AD and MCI subjects.		
	Notes	<ul style="list-style-type: none"> - Automatic identification was performed by segmenting each FDG-PET image and combining those regions (clusters) to obtain a reduced feature space. - Three classifiers were used to accomplish the comparison: SVM, KNN, and naïve Bayes classifier. 		
	Type	-		
	Results	<ul style="list-style-type: none"> - The found regions were automatically very discriminative (when using SVM and KNN) and were better than results with regions defined by experts. - The voxel intensity approach was the one with the lowest accuracy. - Merging the ROIs found by the experts together with the automatic identification of ROIs differentiated between the MCI subjects and AD better than the automatic method using a naïve Bayes classifier. - The highest accuracies were obtained with a lower number of features, and all the approaches decreased their performance when the number of features increased. - KNN was the worst classifier, and Naïve Bayes, in some approaches outperformed SVM. - For classification tasks other than AD vs. MCI, the accuracies became a little higher: for AD vs. NC it could be around or higher than 85%, and for MCI vs. NC, it achieved results between 65% and 79% relying on the used classifier and approach. 		
	Clinical findings	Assisting the experts in the early diagnosis of AD.		
Dataset	ADNI			
Scanning Char.	-			
Brain Region	<p>Voxels regions. <i>Note: for automatically based identification of ROIs, each FDG-PET scan is segmented, getting a partitioning of the image into regions (clusters) using DBSCAN.</i> <i>For expert based identification, seven ROIs were identified namely: lateral temporal (right and left); mesial temporal (right and left); inferior frontal gyrus/orbitofrontal; inferior anterior cingulate; superior anterior cingulate; dorsolateral parietal (right and left); posterior cingulate and precuneus.</i></p>			
Subjects	Group	NC	MCI	AD
	No.	-	59	59
	Age (mean±SD)	-	77.7±6.9	78.3±6.6
System Char.	Two types (automatic/objective and semiautomatic/subjective) were compared			
Ref.	79			
Approach details	Goal	Estimation of the temporal trajectories of voxelwise amyloid (EM algorithm)		
	Notes	-		
	Type	Unsupervised		
	Results	The longitudinal trajectory slopes estimated using the proposed method showed better localized longitudinal changes as compared to regressing on age at each voxel.		
	Clinical findings	The results were consistent across the hemispheres and agree with a global index of brain amyloid known as mean cortical distribution volume ratio (DVR). Unlike mean cortical DVR, which depends on a priori defined regions, the progression score extracted by the method was data-driven and did not make assumptions about regional longitudinal changes.		
Dataset	Longitudinal PET from the Baltimore longitudinal study of aging (BLSA)			
Scanning Char.	PET scans were acquired on a GE Advance scanner immediately following an intravenous bolus injection of PiB, which binds to fibrillar β -amyloid. Dynamic PET data were acquired over 70 min, yielding 33-time frames each with 128×128×35 voxels. Voxel size is 2×2×4.25 mm ³ .			
Brain Region	<p>Temporal trajectories of amyloid deposition <i>Note: each cerebral hemisphere was considered separately</i></p>			
Subjects	Group	NC	MCI	AD
	No.	Data for 75 participants		
	Age	Ages of 55.7–92.4 at baseline were used.		
System Char.	Semiautomatic/Subjective			

integrating continuous attribute discretization along with the AR-mining.

Illán *et al.* (86) proposed a CAD system that relied on the ICA for the purpose of feature extraction and selection. In addition, SVM was used for the purpose of classification. The study performed two classification tasks, represented by two methods: Method I was NC vs. dementia (combining MCI, probable AD, and certain AD in one category) while method II was NC vs. MCI vs. probable AD vs. certain AD. The system achieved an error of estimation under 9% and specificity of 95.12%. On the other hand, the second method showed a high accuracy of 91.1% when training SVM using RBF kernel function. Also, method II showed the highest sensitivity, which more adequately characterizes AD. This finding was supported by some studies that showed the affected regions of the brain, which might be attained by different hypo-perfusion levels through the AD stages. Also, Illán *et al.* proposed a CAD system (87) that relied on mask-based techniques for feature reduction, combined component-based SVM for the classification task, and pasting-votes method of assembling SVM classifiers for final decision making. Two distinct voting methodologies were considered: majority and relevance. The former incorporates all components into the final decision, while the latter uses a subset of components deemed relevant. The results illustrated the better accuracy and reduced computation time with relevance voting when compared to the majority voting method. Regarding classification accuracy, training SVM with RBF kernel function assisted in obtaining an accuracy of 96.91%. In the same context, Illán *et al.* (88) analyzed the importance of the latent brain symmetry and asymmetry parts in the AD subjects' identification. To perform such analysis, they demonstrated a CAD system that relied on eigenspace extension for feature extraction and SVM for classification. The experimental results of the proposed system showed an identification accuracy of 92.78% with the presence of latent symmetry of the brain, linear kernel, and a leave-one-out cross-validation strategy. Although pronounced asymmetries in the hypometabolic patterns were specific to AD, the usage of such to test for AD was not especially sensitive. The study concluded that considering only the symmetric component of the spectrum was relevant to recognizing AD subjects.

Martínez *et al.* (89) proposed a CAD system that serves the early diagnosis of AD through building decision models that provided its decision based on two different classifiers. The difference between these classifiers was in the form of selecting the required voxels where two criteria were used (i.e., Mann-Whitney-Wilcoxon test/relative entropy). These two criteria were used to find different brain regions that may differ from one patient to another.

The classification results achieved 92.78% that was better than other state-of-the-art methods, which were used for comparison. Also, regarding the CAD system that was presented by Martínez-Murcia *et al.* (70), the evaluation of the system on the SPECT database showed an accuracy of 93.7% for the classification task, and thus assisted in the early diagnosis of the disease.

As previously mentioned, López *et al.* (69) proposed a CAD system for early diagnosis of AD. In addition to the general results on PET and SPECT databases, the SPECT images achieved a classification accuracy of 96.7 %.

Segovia *et al.* (90) aimed to improve on existing CAD systems by using a PLS algorithm to extract features for an SVM-based classifier. PLS was used for decomposing the images into scores and loadings. Comparing the obtained features using PLS-based methodology against those achieved by the well-known PCA approach, it showed better FDR results with the PLS-based methodology. Ultimately, the CAD system's classification accuracy achieved results higher than 90%, which was better than other referenced methods. More details regarding the results of SPECT related studies can be found in Table 8.

3.3. Other Modalities

3.3.1. Functional magnetic resonance imaging (fMRI)

fMRI is an MR imaging technique that aims to capture the intrinsic changes of the blood oxygen level-dependent (BOLD) signal (91). fMRI captures the brain region function that is involved in certain cognitive tasks in addition to capturing the general functions of the brain involving speech, language, and sensory motion (14).

Regarding AD, fMRI is used in monitoring the treatment status. Studying both the resting and the activation states of the fMRI indicates the lesser-coordinated activity of the AD patients compared with normal subjects within the hippocampus, inferior parietal lobes, and the cingulate cortex. Additionally, the neural substrate that is related to the behavioral functions or cognition occurs in the early stages of the neurodegenerative disorder. Therefore, correlation of behavioral or cognitive function with the neuroanatomical network has become possible due to recent fMRI advances (14). Figure 8 (92) shows an example of fMRI of NC and AD subjects while performing a task that consists of memorizing a series of faces. As shown by the red color on the figure that represents the increased activity when performing the task, the NC shows higher activation than does the AD subject.

Medical imaging diagnosis of early Alzheimer's disease

Table 8. The SPECT related studies

Ref.	80			
Approach details	Goal	Classification (2D GW (analysis of SPECT) + PCA (feature extraction) + SVM (classification))		
	Notes	- 16 GW sets (scales=2, orientations=6) were applied and found to be enough. - Before applying PCA, FDR was used for the purpose of feature selection from the GW-based images.		
	Type	Supervised		
	Results	- The best results were found to be when the number of used principal components was 3. - The classification of the proposed method achieved up to 96% accuracy. - Improved the classification accuracy results of the PCA+SVM methods.		
	Clinical findings	Assisting the experts in the early diagnosis of AD.		
Dataset	Virgen de las Nieves Hospital (Granada, Spain)			
Scanning Char.	The patients were injected with a gamma emitting 99mTc-ECD radiopharmaceutical, and the SPECT raw data was acquired by a three head gamma camera Picker Prism 3000.			
Brain Region	Function of the brain (rCBF)			
Subjects	Group	NC	MCI	AD
	No.	41	-	56
	Age	-	-	-
System Char.	Automatic/Objective			

Ref.	81			
Approach details	Goal	CAD system (FDR (feature selection), NMF (feature extraction), classification (SVM))		
	Notes	-		
	Type	Supervised		
	Results	The system achieved up to 94.9% of the classification accuracy.		
	Clinical findings	Assisting the experts in the early diagnosis of AD.		
Dataset	Virgen de las Nieves Hospital (Granada, Spain)			
Scanning Char.	The patients were injected with a gamma emitting technetium-99m labeled ethyl cysteinate dimer (99mTc-ECD) radiopharmaceutical, and the SPECT images were captured through a 3-head gamma camera Picker Prism 3000.			
Brain Region	rCBF			
Subjects	Group	NC	MCI	AD
	No.	41	-	56
	Age	-	-	-
System Char.	Automatic/Objective			

Ref.	83			
Approach details	Goal	CAD system (PCA/PLS regression model (downscaling and feature extracting), RF predictor (classification))		
	Notes	-		
	Type	Supervised		
	Results	- When the number of the forest trees increased, the system showed a convergence to a limit in the generalization error. Thus, the reduction in the generalization error occurred when using PLS and depended on the individual forest trees' strength and the existed correlation between them. - PLS feature extraction was found to be more effective for extracting discriminative information from the data than PCA, yielding peak accuracy values of 96.9%.		
	Clinical findings	Assisting the experts in the early diagnosis of AD.		
Dataset	Virgen de las Nieves Hospital in Granada (Spain)			
Scanning Char.	The patients were injected with a gamma emitting 99mTc-ECD radiopharmaceutical, and the SPECT raw data was acquired by a three-head gamma camera Picker Prism 3000.			

Medical imaging diagnosis of early Alzheimer's disease

Brain Region	rCBF				
Subjects	Group	NC	MCI	AD	
	No.	41	30	moderate	Severe
	Age	-	-	22	4
System Char.	Automatic/Objective				
Ref.	84				
Approach details	Goal	CAD system (Welch's <i>t</i> -test (feature selection), linear kernel based SVM/classification trees (classification))			
	Notes	<ul style="list-style-type: none"> - The voxels selection was performed through the <i>t</i>-values that were greater than different thresholds. - Then, the used feature vectors were obtained through the mean and SD of the selected voxels. 			
	Type	Supervised			
	Results	<ul style="list-style-type: none"> - The accuracy of the classification obtained through linear based SVM and classification trees was found to be proportional to the threshold values used for feature selection. - In general, linear based SVM showed higher correct rate than classification trees, except when the values of threshold that are very high. - Other classifiers such as quadratic based SVM, RBF based SVM, and Fisher-linear discriminant analysis were also evaluated for the classification goals. The findings showed that they, in general, had similar performance to the linear based SVM used in this study. - The proposed methodology achieved the best classification accuracy of 96.2% using classification trees. - Regarding sensitivity and specificity, SVM achieved higher sensitivity while the decision trees achieved higher specificity when the threshold values were high. 			
Clinical findings	Classifying the subjects into normal and affected in a parsimonious way without prior knowledge.				
Dataset	-				
Scanning Char.	The patients were injected with a gamma emitting ^{99m} Tc-ECD radiopharmaceutical, and the SPECT raw data were acquired through a camera of three head gamma Picker Prism 3000. Totally, 180 projections were captured for each patient with a 2° angular resolution.				
Brain Region	Function of the brain				
Subjects	Group	NC	MCI	AD	
	No.	41	-	38	
	Age	-	-	-	
System Char.	Automatic/Objective				
Ref.	85				
Approach details	Goal	Classification (VAF and AE (feature extraction), ARs (mining))			
	Notes	-			
	Type	Supervised			
	Results	<ul style="list-style-type: none"> - The study compared the supervised (with the prior goal of 2 most discriminant rules) and unsupervised mode (without any prior goals) of ARs. The experiments showed the same accuracy results for the both modes but better computation time efficiency in the supervised mode. - Achieves classification accuracy of 95.87%. 			
Clinical findings	Assisting the experts in the early diagnosis of AD.				
Dataset	Virgen de las Nieves Hospital in Granada (Spain)				
Scanning Char.	The patients were injected with a gamma ting ^{99m} Tc-ECD radiopharmaceutical, and the SPECT raw data was acquired by a three head gamma camera Picker Prism 3000. A total of 180 projections were taken with a 2-degree angular resolution				
Brain Region	rCBF				
Subjects	Group	NC	MCI	AD	
	No.	43	30	moderate	severe
	Age	-	-	20	4
System Char.	Automatic/Objective				

Medical imaging diagnosis of early Alzheimer's disease

Ref.	82			
Approach details	Goal	CAD system (FDR (data analysis), NMF (feature selection and extraction), SVM (classification))		
	Notes	-		
	Type	Supervised		
	Results	The system achieved classification accuracy up to 94%.		
	Clinical findings	Assisting the experts in the early diagnosis of AD.		
Dataset	Virgen de las Nieves Hospital in Granada (Spain)			
Scanning Char.	Each patient was injected with a gammaemittingtechnetium-99m labeled ethyl cysteinate dimer (99mTc-ECD) radiopharmaceutical, and the SPECT scan was acquired using a 3-head gamma camera Picker Prism 3000.			
Brain Region	rCBF			
Subjects	Group	NC	MCI	AD
	No.	41	-	56
	Age	-	-	-
System Char.	Automatic/Objective			

Ref.	87			
Approach details	Goal	CAD (ICA (feature extraction and selection), SVM (classification))		
	Notes	<ul style="list-style-type: none"> - Two methods were defined: Method I: used two categories: NC and AD (combined the three stages of AD into one category). Method II: used four categories: NC, MCI, probable and certain. - Four SVM-related kernel functions were tested: linear, quadratic, RBF, and polynomial. 		
	Type	Supervised		
	Results	<ul style="list-style-type: none"> - With a small number of features, the non-linear kernel functions generalized better as linear kernel functions. - Method I showed the high specificity performance of 95.12%. - Method II showed high sensitivity. - The best performance of the system was achieved with Method II with an accuracy of 91.1% when combined with RBF kernel. - Regarding features, comparing ICA, PCA and VAF showed the improvement of ICA over the others. - The system caused an error estimation below 9%. 		
	Clinical findings	The high sensitivity of Method II showed that the affected regions of the brain might be attained by different hypo-perfusion levels through the AD stages.		
Dataset	Virgen de las Nieves Hospital in Granada (Spain)			
Scanning Char.	The database produced with an injected gamma emitting 99mTc-ECD radiopharmaceutical and acquired by a three-head gamma camera Picker Prism 3000.			
Brain Region	rCBF			
Subjects	Group	NC	MCI	AD
	No.	41	20	Probable 14 Certain 4
	Age	-	-	-
System Char.	Automatic/Objective			

Ref.	90			
Approach details	Goal	CAD system (Mann-Whitney-Wilcoxon test/Relative Entropy (voxels ranking and selection), factor analysis (feature extraction), multivariate normal classifier (classification))		
	Notes	<ul style="list-style-type: none"> - The final decision was made based on two different classifiers: Classifier A: Mann-Whitney-Wilcoxon test, factor analysis, and multivariate normal classifier Classifier B: Relative Entropy, factor analysis, multivariate normal classifier 		
	Type	Supervised		
	Results	The proposed technique achieved a classification accuracy of 92.78% that was better than other compared methods.		
	Clinical findings	Assisting the experts in the early diagnosis of AD.		
Dataset	Virgen de las Nieves Hospital (Granada, Spain)			
Scanning Char.	-			

Medical imaging diagnosis of early Alzheimer's disease

Brain Region	rCBF				
Subjects	Group	NC	MCI	AD	
	No.	43	30	Probable	Certain
	Age range (mean±SD)	46–85 (71.51±7.99)	23–81 (65.29±13.36)	46–86 (65.73±8.25)	69–83 (76±9.90)
System Char.	Automatic/Objective				

Ref.	88				
Approach details	Goal	CAD system (mask-based techniques (feature reduction), combined component based-SVM (classification), pasting-votes method of assembling SVM classifiers (final decision making))			
	Notes	<ul style="list-style-type: none"> - Two methods for aggregating the votes were proposed: 1-Majority vote: where the final decision was relied on using all the components. 2-Relevance voting: where casting a vote relied on the most relevant components. The relevance of each component was defined as the classifier performance where some wrapper filter method was needed to select the component. - Three kernel functions were tested for training SVM: linear, RBF and polynomial. 			
	Type	Supervised			
	Results	<ul style="list-style-type: none"> - Medium image compression showed optimum performance while high image compression caused detail degradation that in turn decreased the performance. - Relevance voting method showed an accuracy of 89% (with medium compression) which was better than VAF and majority voting methods. Also, relevance voting method showed better computational time compared to the majority voting method. - The system achieved the best accuracy of 96.91% when SVM trained with RBF kernel. 			
	Clinical findings	- Assisting the experts in the early diagnosis of AD.			
Dataset	Virgen de las Nieves' Hospital (Granada, Spain)				
Scanning Char.	The 3D SPECT brain images were produced through an injection with gamma emitting 99mTc-ECD radiopharmaceutical and acquired by a three-head gamma camera Picker Prism 3000.				
Brain Region	rCBF				
Subjects	Group	NC	MCI	AD	
	No.	41	20	Probable	Certain
	Age	-	-	14	4
System Char.	Automatic/Objective				

Ref.	86				
Approach details	Goal	Classification (combine VOF, NMSE, <i>t</i> -test selection and KPCA (feature extraction), Kernel Distance Metric Learning Methods (classification))			
	Notes	-			
	Type	Supervised			
	Results	The study compared Euclidean, Mahalanobis and energy-based distance metric learning for the classification. The Energy-based method achieved 96.91% classification accuracy which represented the highest accuracy among the three tested classifiers.			
	Clinical findings	Assisting the experts in the early diagnosis of AD			
Dataset	Virgen de las Nieves Hospital in Granada (Spain)				
Scanning Char.	The patients were injected with a gammaemitting99mTc-ECD radiopharmaceutical, and a camera of a three head gamma Picker Prism 3000 was used to acquire the SPECT raw data. Totally, 180 projections were acquired with a 2-degree angular resolution.				
Brain Region	rCBF				
Subjects	Group	NC	MCI	AD	
	No.	43	30	Moderate	Severe
	Age	-	-	20	4
System Char.	Automatic/Objective				

Medical imaging diagnosis of early Alzheimer's disease

Ref.	70					
Approach details	Goal	CAD system (PCA/ LDA (feature extraction) + FDR (feature selection) + ANN/SVM (classification))				
	Notes	- The best combination of techniques that composed complete CAD systems was not fixed but depended on the specific database and the classification task they dealt with.				
	Type	Supervised				
	Results	<ul style="list-style-type: none"> - In general, SVM provided better results than ANN with the same features. - When classes were best classified by linear surfaces or decision lines, the rearrangement of the PCA coefficients by the FDR criterion usually yielded higher accuracy rates. - The system achieved a classification accuracy of 96.7%. 				
	Clinical findings	Assisting the experts in the early diagnosis of AD.				
Dataset	Virgen de las Nieves Hospital in Granada (Spain)					
Scanning Char.	-					
Brain Region	rCBF					
Subjects	Group	NC	MCI	AD		
	No.	41	27	Probable	Certain	
				19	4	
Age range (mean±SD)	46–85 (71.51±7.99)	23–81 (65.29±13.36)	46–86 (65.73±8.25)	69–83 (76±9.90)		
System Char.	Automatic/Objective					
Ref.	73					
Approach details	Goal	CAD system (AR-mining and combination (feature selection) + PCA/PLS (feature extraction) + SVM (classification))				
	Notes	-				
	Type	Supervised				
	Results	The classification accuracy achieved results up to 91.75%				
	Clinical findings	Assisting the experts in the early diagnosis of AD.				
Dataset	Virgen de las Nieves Hospital (Granada, Spain)					
Scanning Char.	Note: The images were acquired in the form of PRISM 3000 gamma camera after injecting the subjects by gamma emitting tech-netium-99 m labeled ethyl cysteine dimer (99mTc-ECD).					
Brain Region	rCBF for identifying pathologic anomalies in internal tissues or organs, even before anatomical and structural alterations are observable.					
Subjects	Group	NC	MCI	AD		
	No.	41	30	Moderate	Severe	
				22	4	
Age range (mean±SD)	46–85 (71.51±7.99)	23–81 (65.20±13.36)	46–86 (65.73±8.25)	69–83 (76±9.90)		
System Char.	Automatic/Objective					
Ref.	89					
Approach details	Goal	Exploring the brain latent symmetry importance (CAD system (eigenspace extension (PCA) (feature extraction), SVM (classification))				
	Notes	-				
	Type	Supervised				
	Results	<ul style="list-style-type: none"> - The system achieved an identification accuracy of 92.78% with the latent symmetry of the brain, linear kernel, and a leave-one-out cross-validation strategy. - The usage of asymmetries for the test of the AD was very specific but not especially sensitive. 				
	Clinical findings	<ul style="list-style-type: none"> - Considering just the symmetric part of the spectrum showed an improvement in the AD subject's recognition. - When the asymmetries in the hypometabolic patterns were presented, they were pronounced in the AD subjects. 				
Dataset	Virgen de las Nieves Hospital (Granada, Spain)					

Medical imaging diagnosis of early Alzheimer's disease

Scanning Char.	The 3D SPECT brain images were acquired through an injection with gamma emitting 99mTc-ECD radiopharmaceutical and acquired by a three-head gamma camera Picker Prism 3000.				
Brain Region	rCBF				
Subjects	Group	NC	MCI	AD	
	No.	41	30	Moderate	Severe
	Age range (mean±SD)	46–85 (71.51±7.99)	23–81 (65.2±13.36)	46–86 (65.73±8.25)	69–83 (76±9.90)
System Char.	Automatic/Objective				
Ref.	71				
Approach details	Goal	CAD system (voxel selection (Mann–Whitney–Wilcoxon U-Test), feature extraction (Factor Analysis) and classification (linear SVM))			
	Notes	<ul style="list-style-type: none"> - Using Mann–Whitney–Wilcoxon selection criteria for the purpose of voxel selection represented one of the strengths of the proposed system since it prevented the system from selecting outliers. - The purpose of proposing the factor analysis was to extract common factors and factor loadings from the selected voxels and thus help in carrying out the feature reduction. 			
	Type	Supervised			
	Results	The classification accuracy achieved 93.7%.			
	Clinical findings	Assisting the experts in the early diagnosis of AD.			
Dataset	Virgen de las Nieves Hospital in Granada (Spain)				
Scanning Char.	-				
Brain Region	rCBF				
Subjects	Group	NC	MCI	AD	
	No.	41	29	Probable	Certain
	Age range (mean±SD)	46–85 (71.51±7.99)	23–81 (65.2±13.36)	46–86 (65.7±8.25)	69–83 (76±9.9)
System Char.	Automatic/Objective				
Ref.	74				
Approach details	Goal	CAD system (data analysis (FDR)+feature selection and extraction (NMF) + classification (SVM with bounds of confidence))			
	Notes	Three different approaches for the classifier were provided and detailed, two of them included bounds of confidence and took advantage of the definition of a "security region" in the SVM hyperplane, where no decision was assumed.			
	Type	Supervised			
	Results	The system achieved up to 91% of the classification accuracy.			
	Clinical findings	Assisting the experts in the early diagnosis of AD.			
Dataset	Virgen de las Nieves Hospital in Granada (Spain)				
Scanning Char.	Each patient was injected with a gamma emitting technetium-99m labeled ethyl cysteinate dimer (99mTc-ECD) radiopharmaceutical, and the SPECT images were acquired by means of a 3-head gamma camera Picker Prism 3000.				
Brain Region	rCBF				
Subjects	Group	NC	MCI	AD	
	No.	41	-	56	
	Age	-	-	-	
System Char.	Automatic/Objective				

Medical imaging diagnosis of early Alzheimer's disease

Ref.	72					
Approach details	Goal	CAD system (FDR and AE (feature/ROI extraction), AR (mining))				
	Notes	<ul style="list-style-type: none"> - The FDR was used to enable the selection of the discriminant regions for further analysis and to reduce the computational cost. - AE provided a trade-off between the computation complexities, the accuracy of the image classification, and allowed all relevant brain regions to be included. 				
	Type	Supervised				
	Results	The system achieved an accuracy of 92.78%				
	Clinical findings	Assisting the experts in the early diagnosis of AD.				
Dataset	Virgen de las Nieves Hospital in Granada (Spain)					
Scanning Char.	Each subject was injected with a gamma emitting technetium-99 m labeled ethyl cysteinate dimer (99mTc-ECD) radiopharmaceutical, and the SPECT scan is acquired by means of a 3-head gamma camera Picker Prism 3000.					
Brain Region	rCBF					
Subjects	Group	NC	MCI	AD		
	No.	42	30	Probable	Certain	
				21	4	
Age	-	-	-	-		
System Char.	Automatic/Objective					
Ref.	14					
Approach details	Goal	CAD system (continuous attribute discretization (feature selection) + AR mining (classification))				
	Notes	Image histogram segmentation was used over the mean control images to obtain the best mask that in turn was used in the feature selection step.				
	Type	Supervised				
	Results	Obtained classification accuracy up to 96.91%				
	Clinical findings	Assisting the experts in the early diagnosis of AD.				
Dataset	Virgen de las Nieves Hospital (Granada, Spain)					
Scanning Char.	Note: The images were acquired in the form of PRISM 3000 gamma camera after injecting the subjects by gamma emitting tech-netium-99 m labeled ethyl cysteinate dimer (99mTc-ECD).					
Brain Region	rCBF for identifying pathologic anomalies in internal tissues or organs, even before anatomical and structural alterations are observable.					
Subjects	Group	NC	MCI	AD		
	No.	41	30	Moderate	Severe	
				22	4	
Age range (mean±SD)	46–85 (71.51±7.99)	23–81 (65.20±13.36)	46–86 (65.73±8.25)	69–83 (76±9.90)		
System Char.	Automatic/Objective					
Ref.	91					
Approach details	Goal	1-Feature extraction method (PLS) 2-CAD system (PLS regression model (feature extraction), Out-Of-Bag error (feature selection), SVM (classification))				
	Notes	-				
	Type	Supervised				
	Results	<ul style="list-style-type: none"> - The features obtained through PLS showed better FDR when compared with the PCA approach. - The system achieved a classification accuracy of 91.6%, the sensitivity of 92.7% and specificity of 91.1%. 				
	Clinical findings	Assisting the experts in the early diagnosis of AD.				
Dataset	Virgen de las Nieves Hospital in Granada (Spain)					
Scanning Char.	The patients were injected with a gamma emit-ting99mTc-ECD radiopharmaceutical and the SPECT raw data was acquired by a three head gamma camera Picker Prism 3000. A total of 180 projections were taken with a 2° angular resolution.					
Brain Region	rCBF					
Subjects	Group	NC	MCI	AD		
	No.	41	30	Moderate	Severe	
				22	4	
Age range (mean±SD)	46–85 (71.51±7.99)	23–81 (65.86±13.36)	46–86 (65.73±8.25)	69–83 (76±9.90)		
System Char.	Automatic/Objective					

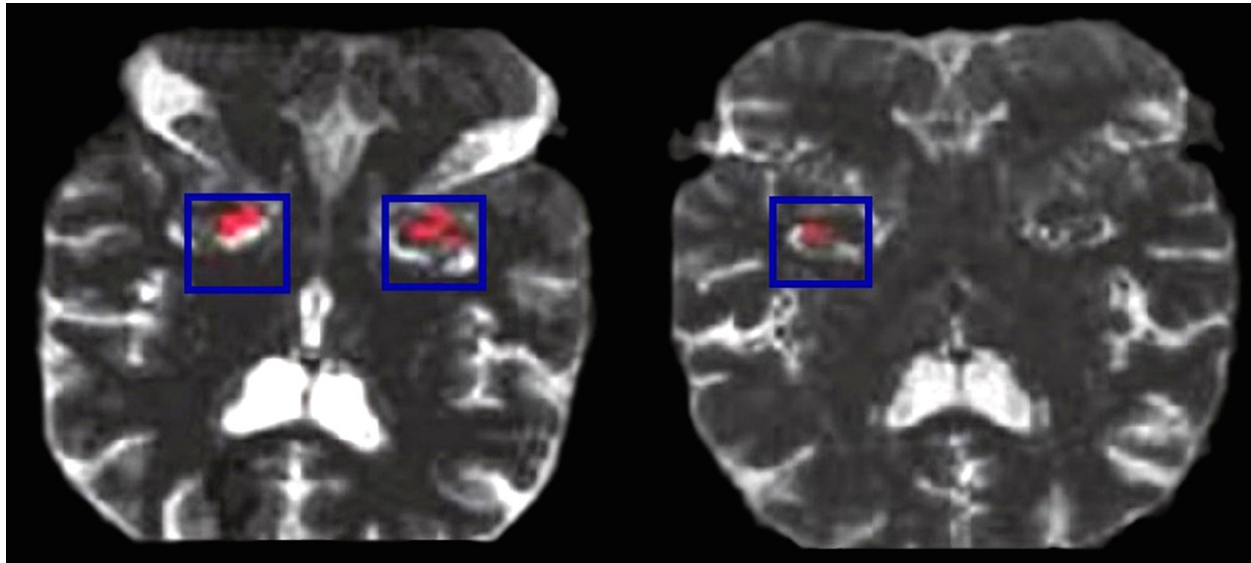


Figure 8. NC and AD subjects' fMRI scans performing an activation task (93), memorizing faces, with the red color areas in the blue rectangles represent the fires when performing the required task.

For the early diagnosis of AD, Hu *et al.* (93) dealt with functional connectivity between different regions of the brain by utilizing fMRI scans to help in the early stages' prediction of AD. Their experiments showed that functional connectivity between brain regions is of more importance than activity within regions in predicting cognitive decline.

In the same context, Challis *et al.* (94) worked with the functional connectivity of the brain from the resting state fMRI (rsfMRI) to stratify between NC, aMCI, and AD subjects. This study achieved good classification results even without including information on focal atrophy. A detailed illustration of fMRI-related studies is presented in Table 9.

3.3.2. Diffusion tensor imaging (DTI)

DTI is a modality built upon MRI, applying diffusion-weighted pulse sequences with magnetic field gradients in at least six different directions and possibly of different magnitudes to produce MRI signals characterized by the sensitivity to the random microscopic motion of water. The purpose of DTI is to estimate the tensor that characterizes diffusion of water within brain tissue, which provides the ability to study the microstructure of the white matter and the fiber pathways (tractography) between brain regions (95). The symmetric, second rank diffusion tensor is often reduced to four scalar or pseudoscalar summary statistics: axial diffusivity (ADT), radial diffusivity (RD), mean diffusivity (MD), and fractional anisotropy (FA) (96). Such results assist in measuring as well as quantifying the orientation of the tissues. In addition, their structure assists in the examination process of cerebral WM as well as the neural fiber tracts.

As an example, Figure 9 (97), shows a comparison between AD and NC subjects that, according to the studies, shows the increased MD in addition to decreased FA in the AD as compared to NC (97). For more details, related to the DTI and its mechanism of work, please see (78).

Regarding AD, measurement of the fiber tract integrity through DTI helps in a directly assessing the WM fibers. Therefore, it could potentially be considered as an AD biomarker. In addition, it reflects any disruption in the axons through random movement of water molecules through the tissues. Therefore, it helps in characterizing AD since such disruption causes, in turn, a reduction in the anisotropy. In other words, the water molecules' movement along the neural tract length is greater than those across tract width. Finally, the regional analysis of the DTI shows that the changes in the hippocampal microstructure may represent a better indicator of the MCI progression risk to AD (26).

For early diagnosis of AD, Wee *et al.* (98) relied on a collection of measures obtained from the connectivity networks of the WM to help in distinguishing MCI and NC subjects through presenting a classification algorithm. They worked on presenting enriched WM connections that were described through the use of six physiological parameters: fiber penetration count, FA, MD, and principal diffusivities ($\lambda_1, \lambda_2, \lambda_3$). Such utilization associated each subject with six connectivity networks to account for both connection topology and biophysical properties. To help in the accurate detection of MCI, the study selected certain brain regions and presented them to the classification step. These regions included

.Table 9. The fMRI-related studies

Ref.	94			
Approach details	Goal	Classification (auto-encoder architecture)		
	Notes	-		
	Type	Supervised		
	Results	The experiment results showed that the proposed method found the correlations between different brain regions efficiently, and provides a strong reference for AD prediction. Compared to SVM, about 25% improvement was gained through the proposed work in the prediction accuracy.		
	Clinical findings	The connections between brain regions showed more importance than the pure function of the regions and that the cognitive ability of people heavily depended on this.		
Dataset	ADNI			
Scanning Char.	The DICOM fMRI data was scanned by the 3.0. Tesla Philips medical system. Flip angle = 80; repetition time (TR) = 3000 ms; echo time (TE) = 30 ms; pixel size = 3.3. × 3.3.; slice thickness = 3.3. mm; matrix size = 64 × 63. More information about the resting state parameters can be found on the website of ADNI.			
Brain Region	Brain functional connection			
Subjects	Group	NC	MCI	AD
	No.	52	48	-
	Age (range)	63.2 - 88.3	66.5 - 87.3	-
System Char.	Automatic/Objective			
Ref.	95			
Approach details	Goal	Patient stratification (Bayesian GP logistic regression (GP-LR) models with linear and non-linear covariance functions)		
	Notes	-		
	Type	Supervised		
	Results	The results supported the hypothesis that Bayesian GP-LR models can be effective at performing patient stratification: the implemented model achieved 75% accuracy disambiguating NC from subjects with aMCI and 97% accuracy disambiguating aMCI subjects from those with AD. Accuracies were estimated using a held-out test set. Both results were significant at the 1% level.		
	Clinical findings	Assist in the early diagnosis of AD.		
Dataset	Data are available upon request			
Scanning Char.	All subjects underwent a MRI examination at 3 T (Siemens, Medical Solutions, Erlangen, Germany), including the following acquisitions: 3D modified driven equilibrium Fourier transform (MDEFT) scan (TR = 1338 ms, TE = 2.4. ms); and T2* weighted echo planar (EPI) sensitised to BOLD contrast (TR = 2080 ms, TE = 30 ms, 32 axial slices, matrix = 64 × 64, pixel size = 3 × 3 mm ² , slice thickness = 2.5. mm, flip angle: 70°) for rsfMRI. BOLD EPIs were collected during rest for a 7 minute and 20 second period, resulting in a total of 220 volumes. During this acquisition, subjects were instructed to keep their eyes closed, not to think of anything in particular and not to fall asleep.			
Brain Region	Functional connectivity patterns of the brain			
Subjects	Group	NC	MCI	AD
	No.	39	aMCI: 50	27
	Age (mean±SD)	63±9	66±7	68±6
System Char.	Automatic/Objective			

the rectus gyrus region within the orbital portion of the frontal lobe and the insula within the lateral fissure between the temporal lobe and the frontal lobe. The experiments showed that relying on the connection topology and biophysical properties revealed more relevant and subtle information that, in turn, serves the purpose of classification.

Schwab *et al.* (99) incorporated DTI into a diagnostic framework combining automated feature

selection, registration, and atlas construction. They focused on the beta-amyloid (Aβ) pathology of AD and its relationship to the degenerative changes reflected in the neuroanatomy. The study found a high probability of association between the presence of amyloid deposits and features of the parahippocampal WM, in that feature intensity was reduced in that region for Aβ+ cases compared with Aβ-. More details regarding DTI studies are found in Table 10.

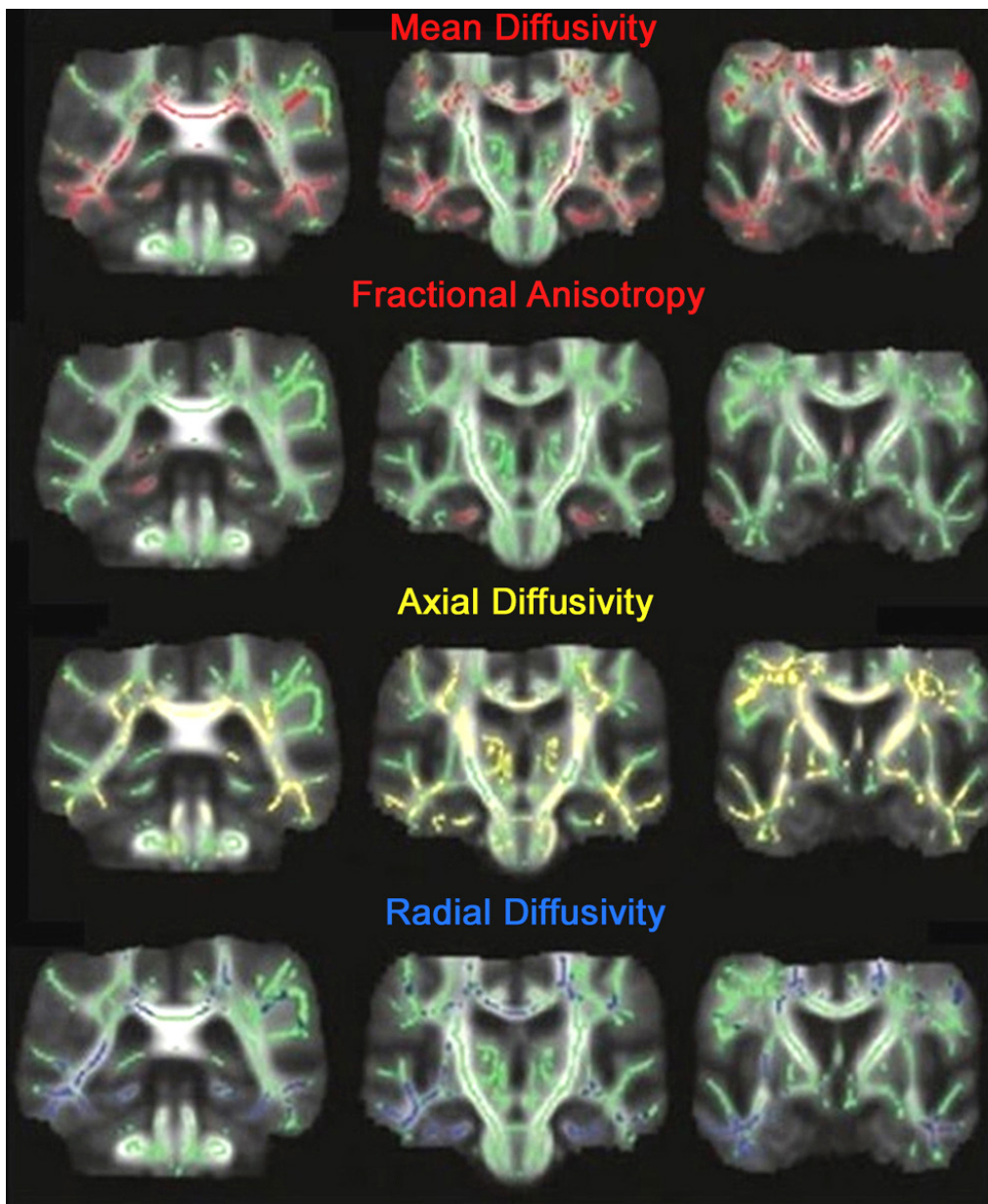


Figure 9. Example (98) of abnormalities between AD as well as NCs subjects. The spatial statistical tract color maps that represent the differences of the voxels between the subjects are overlaid on the mean FA skeleton. The red color indicates the voxels with increased MD and decreased FA. Yellow color represents voxels of increased ADT while the blue color indicates voxels of increased RD.

3.4. Fusion related studies

In addition to the previous studies that relied on information obtained from single modality, various studies combined different sorts of information from various imaging modalities. Such fusion aims to produce more informative results that consequently could assist in the early diagnosis process of AD. For instance, Polikar *et al.* (100) introduced a decision fusion based approach that combined electroencephalogram (EEG), MRI, and FDG-PET data using an ensemble of classifiers. The study

showed, in general, better performance as compared with obtained results when working only with a single modality.

Kanel *et al.* (101) utilized Freesurfer image analysis tools to obtain different volumetric measurements of the hippocampus subfields that consequently helped in classifying the subjects into different AD stages. The study found that involving the hippocampus subfields and raphe nuclei in AD show very different measurements than normal aging with various degeneration rates. In the end,

Table 10. DTI related studies for early diagnosis of AD

Ref.	99			
Approach details	Goal	Classification (SVM)		
	Notes	The key of the proposed classification framework involved an enriched description of WM connections utilizing six physiological parameters: fiber penetration count, FA, MD and principal diffusivities (λ_1 , λ_2 , λ_3)		
	Type	Supervised		
	Results	The classification accuracy by the proposed framework (with six parameters) was 92.6%, which was at least an 18.5% increment from that using any single physiological parameter		
	Clinical findings	<ul style="list-style-type: none"> - The WM connections' topology and biophysical properties revealed more relevant and subtle information that in turn served the purpose of classification - For the classification, the selected brain regions were: the sectus gyrus, which resides on the orbital portion of the frontal lobe, and the insula, lies within the lateral fissure between the temporal lobe and the frontal lobe. These regions represented discriminant features that helped in an accurate detection of MCI. 		
Dataset	Duke-UNC Brain Imaging and Analysis Center, North Carolina, USA			
Scanning Char.	3.0. Tesla scanner (GE Signa EXCITE, GE Healthcare) DWI of each participant were acquired axially parallel to the anterior and posterior commissures (AC-PC) line with 25-direction diffusion-weighted whole-brain volumes using diffusion weighting values, $b = 1000$ s/mm ² , flip angle = 90°, TR = 17 s and TE = 78 ms. The imaging matrix was 128×128 with a rectangular FOV of 256 × 256 mm ² , resulting in a voxel dimension of 2 × 2 × 2 mm ³ . A total of 72 contiguous slices were acquired.			
Brain Region	WM connectivity networks <i>Note: The most discriminant regions that were selected for classification included the rectus gyrus which is located on the orbital portion of the frontal lobe and the insula which is located within the lateral fissure between the temporal lobe and the frontal lobe.</i>			
Subjects	Group	NC	MCI	AD
	No.	10	17	-
	Age (mean ± SD)	74.2 ± 8.6	72.1 ± 8.2	-
System Char.	Semi-automatic/Subjective			
Ref.	100			
Approach details	Goal	Joint feature selection, registration and atlas building framework (Generalized multi-channel large deformation diffeomorphic metric mapping (LDDMM) algorithm)		
	Notes	The proposed framework was applied for the characterization of A β pathology for the early diagnosis of AD. This aimed to a better understanding of the relationship between A β pathology and degenerative changes in neuroanatomy.		
	Type	-		
	Results	The presence of A β pathology (A β +) may be associated with feature decreases in the parahippocampal WM ROI, indicating levels of degradation as compared to a healthy average (A β -).		
	Clinical findings	<ul style="list-style-type: none"> - Association probability between the presences of (Aβ) pathology (Aβ+) and the decrease of the feature in the parahippocampal WM. - These findings, in turn, indicated degradation levels as compared to health average (Aβ-). 		
Dataset	Hippocampal connectivity Project (HCP) at the center for imaging of neurodegenerative diseases (CIND) at the University of California San Francisco (UCSF).			
Scanning Char.	For each subject, 3 high angular resolution diffusion imaging (HARDI) scans were acquired on a Siemens 4T scanner (128 gradient directions, 3 b0 values, FOV: 192, number of slices: 26, resolution: 1.5 mm isotropic, b-value: 1400 s/mm ² , TR/TE: 3500/86, 3n _{ex} averaged to enhance SNR, total protocol time: 1.35 h).			
Brain Region	A β WM pathology <i>Note: Focused on features within the Parahippocampal WM</i>			
Subjects	Group	A β -	A β +	
	No.	15	17	
	Age (mean ± SD)	-	-	
System Char.	Automatic/Objective			

the study mentioned that more systematic studies were required with optimal intrinsic features using the measurements of subfields to achieve early AD diagnosis.

Zhang *et al.* (102) proposed a multi-modal multi-task (M3T) learning scheme for the purpose of joint prediction of multiple variables from multi-modal data through multi-task feature selection (MTFS) and

multi-modal SVM for classification/regression. To achieve that, the study used data of MRI, PET, and CSF in addition to a clinical score of MMSE and ADAS-Cog. To evaluate the performance of the proposed scheme, the study performed two experiments. The first experiment examined the estimation of the MMSE and ADAS-Cog clinical scores in addition to one class label (i.e., AD, MCI, or NC). The second experiment predicted the 2-years changes of MMSE and ADAS-Cog scores beside the conversion of MCI to AD. Both experiments showed better results through the proposed learning scheme than through the compared learning methods.

Kim *et al.* (103) utilized the integration concept to serve the early detection of AD through focusing on different features that could be estimated from the MRI and PET. The experimental results evaluated different aspects. The results revealed that integrating metabolism features (measured from FDG-PET) and volume/thickness features (measured from the MRI) gave the best results. Comparing the proposed method against SVM mainly showed better results of the proposed method when working with volume/thickness measures.

Suk and Shen (104) utilized the deep learning concept to perform a feature representation process of the proposed classification method that finally performed the classification task using multi-kernel (MK) SVM. To test the system, three binary classification problems were considered, AD vs. NC, MCI vs. NC, and MCI-C vs. MCI-NC. The test showed performance accuracies of 95.9%, 85.0%, and 75.8%, respectively. Regarding MCI-C vs. MCI-NC, the system could improve the performance by 4.0%, which is significant for early diagnosis purposes.

Jie *et al.* (105) proposed a manifold regularized multitask feature selection (M2TFS) model using MRI and PET data to improve classification accuracy and consequently assist in the early diagnosis of AD. Two regularization items were included: Group Lasso regularizer was used to select a small number of features across different modalities jointly. Laplacian regularization term, the second item, was used to preserve the whole data related to geometric distribution information from each modality. Testing the proposed model under the supervised task showed better accuracy and sensitivity results as compared with other methods where the accuracy achieved was 95.03%, 79.27%, and 68.94% for classification problems of AD vs. NC, MCI vs. NC, and MCI-C vs. MCI-NC, respectively. Under the semi-supervised task, the results revealed that the proposed model could lead to better discriminant feature selection using the geometric distribution of the data. This finding reflected on the accuracy of the classification that improved

consistently with the increment in the unlabeled samples on the three groups of classifications.

Suk *et al.* (106) attempted to enhance the AD/MCI diagnosis performance through presenting feature representation and multimodal fusion of MRI and FDG-PET to serve the diagnosis process of AD/MCI. The study relied on deep learning for a self-taught system that efficiently combines complementary information from MRI and PET modalities to construct representations. The findings showed better results of the proposed method in various quantitative metrics with other compared methods. Also, by visually inspecting the trained model, the proposed method could discover the complex latent patterns hidden in MRI and FDG-PET in a hierarchical manner. Finally, due to the better results obtained through the proposed method as compared to competing methods, the authors concluded that deep learning sheds new light regarding the analysis of the neuroimaging data. Then, Suk *et al.* (108) utilized the stacked autoencoders (SAE) to perform a feature representation using MRI, FDG-PET, and CSF data. The main motivation was the possibility of the existence of hidden or latent high-level information inherent in the original low-level features that could assist in building a robust model of the diagnosis. The evaluation regarding binary classification problems of AD vs. NC, MCI vs. NC, AD vs. MCI, and MCI-C vs. MCI-NC showed accuracies of 98.8%, 90.7%, 83.7%, and 83.3%, respectively. Also, the unsupervised characteristic of the pre-training in deep learning helped in discovering general latent feature representations that consequently led to classification accuracy enhancement.

Li *et al.* (108) utilized the deep learning concept to help in predicting missing patterns of the PET images on MR images. The process was accomplished through using MRI as input to the model, while the PET would be predicted as the output. The experiments test multiple things: 1) the PET related prediction ability, 2) the classification accuracy compared with other methods, and 3) the impact of the combination of the PET and MRI images features in the accuracy. The results indicated the successful ability of the proposed system to perform the prediction process of PET missing patterns that could improve the diagnosis accuracy. Testing the classification accuracy through MRI, true and predicted PET, and MRI + PET images were performed. In general, the proposed method showed better results compared with other related methods. Also, there were comparable results between predicted PET and true PET. Finally, the combination of PET and MR images features also helped in improving the obtained performance.

Liu *et al.* (109) utilized the deep learning concept to present a CAD system that was helpful in the early diagnosis of AD. The proposed system

used sparse SAE for the representation of the original input while the softmax regression layer was used to perform the classification task. Evaluating the system against single-kernel SVM (SK-SVM) and multi-kernel SVM (MK-SVM) showed better sensitivity results in two binary classification problems, AD vs. NC and MCI vs. NC. For the accuracy, although the proposed system achieved better accuracy in AD vs. NC case, MK-SVM showed better accuracy in the MCI vs. NC problem. Additionally, the classification performance of 4-way classification problems, NC, MCI-C, MCI-NC, and AD using "one against all" approach was evaluated. The SAE/softmax method outperformed SVM in the classification of NC, MCI-NC, and AD while SVM showed better results with regard to the MCI-NC problem. This led to the proposed system having, in general, greater accuracy than SVM on the four-way classification. Then, Liu *et al.* (110) utilized the architecture of deep learning to suggest a diagnostic framework that was capable of distinguishing four AD progression stages with fewer requirements of prior clinical knowledge. The framework utilized SAE to obtain high-level features of the input in an unsupervised fashion. In addition, the framework used zero-masking strategy in the presence of the multimodal data for the purpose of extracting the complementary information from these modalities. For the classification task, although the extracted features of the unsupervised network could be transferred to conventional classifiers (e.g., SVM), the softmax logistic regression was applied. The purpose of such selection of the softmax logistic regression was to utilize the fine-tuning of it in jointly optimizing the entire network. The framework showed better evaluation results as compared to state-of-the-art SVM-based methods as well as to other deep learning frameworks.

Shi *et al.* (111) attempted to serve the identification process of AD/MCI against NC through presenting two strategies: nonlinear feature transformation and feature fusion strategies. Regarding data fusion, the authors examined the fusion process of certain features extracted from MRI. These features were cross-sectional features represented through GM tissue densities and longitudinal features represented through deformation magnitudes (DM). The experiments showed that the proposed strategies gave better results when compared to state-of-the-art solutions. Better performance was obtained using fusion rather than each feature individually.

Li *et al.* (112) proposed a classification model for early diagnosis of AD through fusing MRI, PET, and CSF data along with two clinical scores of each patient, MMSE, and ADAS-Cog. Also, the model utilized the deep learning concept in the form of dropout technique to model the required weights. The reason for choosing dropout method was its ability to improve the generalization capability of the model. Other

components of the model included PCA for feature extraction, stability selection technique, least absolute shrinkage and a selection operator (Lasso) method for feature selection, and SVM for classification. The system achieved the best performance in diagnosing AD with 91.4%, MCI with 77.4%, and diagnosing AD vs. MCI with 70.1%. In the diagnosis of MCI-C vs. MCI-NC, the PCA was found to degrade the results slightly from 58.1% to 57.4%. Identifying the impact of each of the model components showed the largest impact through dropout component, followed by multitasking learning, then stability selection, and ending with PCA. They suggested that the deep traditional learning could not extract information efficiently from small datasets unless a regularization technique, such as dropout, was used. Finally, they found that the dropout technique helped in improving the classification accuracy by 5.9% more than the classical deep learning methods.

Zhang *et al.* (113) proposed a prediction model based on extreme learning machine algorithms (ELMs) for the identification of MCI relying on MRI, PET, and CSF data. First, the study evaluated the complementary nature of the three biomarkers through testing an ELM prediction based model for each biomarker individually, as well as when they were combined. The results, in general, showed better accuracy with the combination. Then, the comparison of the combined model with the SVM and SVM-fusion revealed a better accuracy of the proposed model, but with a slightly better sensitivity when using the SVM.

Cheng *et al.* (114) focused on the classification of MCI-C and MCI-NC subjects through presenting multimodal manifold-regularized transfer learning (M2TL) method with an optimization algorithm for objective function solution. It is noteworthy that the study utilized samples from different domains (i.e., AD/NC), as an auxiliary domain, in a transfer learning manner to help in the discrimination task of MCI-C and MCI-NC, as a target domain. Due to the distribution differences of the auxiliary and target domains, the study utilized maximum mean discrepancy (MMD) criterion and a similarity/dissimilarity measure between two samples from different domains. The study designed a cross-domain Laplacian matrix to reflect the relation among the samples of the target domain, auxiliary domain, and the unlabeled samples. Finally, in the objective function, a group sparsity constraint was used to help in the informative sample selection to predict the labels of the target class. The testing of the proposed method showed that the maximum accuracy of 80.1% of MCI conversion prediction helped in the early diagnosis of AD. Additionally, Cheng *et al.* (115) presented a multimodal multi-label transfer learning (MDML) method. The method was used for transfer learning and multi-label learning for feature selection, MK-SVM for classification, and MK

relevance vector regression machine for regression. Testing classification results of MCI-C vs. MCI-NC showed better results of the proposed method against compared methods. The proposed method achieved accuracies of 73.2%, 70.0%, and 78.7% when testing the results with different modalities (MRI, PET, MRI+PET+CSF), respectively. Additionally, the study tested the prediction of the clinical scores (i.e., MMSE/ADAS-Cog) using different modalities (MRI, PET, MRI+PET+CSF). The tests showed better prediction results than the compared methods. It is noteworthy that the proposed MDML method performed the prediction without a related learning domain. About clinical findings, the method could successfully find the most discriminant regions of the brain (e.g., hippocampal, amygdala, temporal lobe, precuneus, and insula). More details regarding the fusion based studies can be found in Table 11.

4. CHALLENGES AND FUTURE TRENDS

Despite the availability of several scientific efforts that aim to clarify the ambiguity surrounding the early diagnosis of AD, some limitations are still faced by the scientific community that works in this research area. These limitations are related to different factors, such as the available databases that are utilized for testing the proposed methods, the available technologies that produce the medical images/biomarkers, the subjects who are the target of the proposed works, and the applied methods and techniques. The purpose of this section is to highlight the major obstacles that still stand in front of the achievements regarding the research area of the early diagnosis of AD (116).

4.1. Databases

Different databases have emerged to serve the scientific community who work in the AD research field. The existing repositories still face some limitations that affect the scientific development in this area. These limitations include, for example, the absence of useful modalities within these repositories (e.g., EEG, SPECT) and microscopy images. This omission prevents the ability to utilize powerful data mining and other techniques to perform further studies on these modalities along with the other available modalities (e.g., MRI).

In addition to the absence of various modalities, most databases offer MR imaging modality for scientific research. Of course, the availability of MRI is important due to the significant role of this modality in the context of AD as previously mentioned. However, as implied in the previous survey's tables, this trend directs studies to work only in one direction (i.e., to deal with MRI only) and to avoid dealing with other modalities.

In general, most available data are unimodal, with an absence of different modalities in the same subjects that hinder certain processes, such as fusing the multimodal images/data to achieve maximum performance results. In addition, most of the available records are in elderly patients, 55 years of age and older. Consequently, it prevents the analysis of data on younger people who are also at risk of suffering from AD. The number of young people affected by early-onset AD is small but non-negligible, and building databases for the study of this rare condition should be a research priority.

4.2. Modalities

Despite there being significant sources of information on different imaging technologies, there still exist limitations associated with these modalities. For example, PET technology provides high-quality results, but it uses ionizing radiation which can adversely affect human health. MRI, while generally safer, is more costly and cannot be used on patients with metallic implants. These limitations can be circumvented to some degree, but only by sacrificing image quality and further raising costs.

On the other hand, some modalities fail in the process of differentiating between AD and other disorders, which in turn affects the decision-making processes. In addition, some modalities fail to help in the early diagnosis of the disease, although they can assist in subsequent diagnostic stages. Fortunately, advances in medical imaging technologies continue to provide improvements for research and development in overcoming present limitations.

4.3. Applied Techniques

Various methods and techniques are still utilized for deciphering the AD-related diagnostic staging complexity to assist experts in their decision making. Various studies using different techniques have achieved significant results in analyzing AD stages. However, these techniques face limitations that prevent them from being generalized and applied clinically.

Both performance quality and accuracy are considered essential factors, especially in medical applications since any mistake may endanger human life. Although various methods achieve high quality and accuracy results, they are in need of much more research before they are applied in clinical practice.

Besides performance quality and accuracy, the computation time is also a vital factor in real applications. It is an obstacle in front of the implementation of some techniques that, although producing acceptable results, are impractical in a clinical due to their relatively high computation time.

Table 11. The Fusion related studies

Ref.	101			
Approach details	Goal	Decision fusion approach (ensemble of classifiers)		
	Notes	-		
	Type	Supervised		
	Results	10%-20% improvement compared with results obtained through the individual source of data.		
	Clinical findings	The usage of different measures of each modality (electrophysiological vs. anatomical vs. metabolic) helped in obtaining better performance results than those obtained from individual sources of data.		
Dataset	-			
Fused Modalities	MRI, FDG-PET, and EEG			
Scanning Char.	EEG: The event-related potential (ERPs) were captured through the protocol of an auditory oddball paradigm. Electrodes were placed according to 10–20 standard, whose impedances were kept under 20Ω. The patients were tested for 30 minutes with approximately 3 rest minutes for every 5 testing minutes. Random stimuli of 1,000 were presented, 65% consisting of 1 kHz standard tones, 20% as 2 kHz target tones, and 15% of novel sounds. A random 1.0 to 1.3 seconds inter-stimulus interval was inserted. Standard and target stimuli were presented in 100ms busts with a 5ms on/offset envelope. The novel stimuli were environmental sounds that long for about 200ms where each was never repeated and was unique. The subjects were instructed for pressing a button only whenever they heard the target tone. A sampling at 256 samples/s was performed on the data.			
Brain Region	MRI: volumetric measurement of the brain (To consider the brain related volumes' changes) FDG-PET: glucose metabolism of the brain (to measure Hypometabolism (the brain related drop in the metabolic activity)) EEG: ERPs			
Subjects	Group	NC	MCI	AD
	No.	36	-	37
	Age (mean)	71.2	-	74.5
System Char.	Automatic/Objective			
Ref.	102			
Approach details	Goal	Volumetric segmentation (Freesurfer tool)		
	Notes	-		
	Type	-		
	Results	-		
	Clinical findings	The hippocampus subfields and raphe nuclei showed very different measurements from normal aging with different degeneration rates.		
Dataset	ADNI			
Fused Modalities	fMRI, MRI, and PET			
Scanning Char.	-			
Brain Region	fMRI and MRI images: subfields of the hippocampus MRI and PET scans: the raphe nuclei			
Subjects	Group	NC	MCI	AD
	No.	-	-	-
	Age	-	-	-
System Char.	Automatic/Objective			
Ref.	103			
Approach details	Goal	Joint prediction of multiple variables from multi-modal data (MTFS, Multi-modal SVM(classification/regression))		
	Notes	-		
	Type	Supervised		
	Results	The study performed two types of experiments. The first experiment was estimated the MMSE and ADAS-Cog clinical scores in addition to one class label (i.e. AD, MCI, or NC). On the other hand, the second experiment dealt with predicting the 2-year changes of MMSE and ADAS-Cog scores besides the conversion of MCI to AD. Both experiments were based on ADNI baselines MRI, FDG-PET, and CSF data. The results of both experiments showed better results through the proposed learning scheme than the compared learning methods.		
	Clinical findings	Assisting the experts in the early diagnosis of AD.		

Medical imaging diagnosis of early Alzheimer's disease

Dataset	ADNI				
Fused Modalities	MMSE, ADAS-Cog, MRI, PET and CSF data				
Scanning Char.	MRI: were acquired from 1.5 T scanners. PET: were acquired 30–60 min post-injection. CSF: were collected in the morning after a fast for overnight by a needle of 20- or 24-gauge spinal, frozen within 1 collection hour, and transported on dry ice to the University of Pennsylvania Medical Center for the ADNI Biomarker Core laboratory.				
Brain Region	MRI: GM tissue volume PET: average intensity CSF: $A\beta_{42}$, t -tau, and p -tau.				
Subjects	Group	NC	MCI	AD	
	No.	50	MCI-C 43	MCI-NC 48	45
	Age (mean±SD)	75.3 ± 5.2	75.8 ± 6.8	74.7 ± 7.7	75.4 ± 7.1
System Char.	Automatic/Objective				
Ref.	104				
Approach details	Goal	Classification using automatic whole-brain ROI analysis techniques and Graph-based semi-supervised learning (SSL) method for multimodal brain imaging data integration			
	Notes	The utilized brain imaging data that were used as features were (voxel-based morphometry (VBM) and FreeSurfer V5) and PET (FDG and Florbetapir) scans.			
	Type	Semi-supervised			
	Results	<ul style="list-style-type: none"> - Evaluating the integration effort showed the following results: 1-The integration of FDG and FreeSurfer showed the best performance 2-The integration of Florbetapir and VBM was better than using VBM only. 3-The integration of the four types of brain imaging data did not show the best results. - Comparing the proposed (graph-based SSL) method with SVM showed that the proposed method obtained better results in general except for Florbetapir data. Note: Among the compared datasets, significantly better results were obtained using FreeSurfer dataset. 			
	Clinical findings	<ul style="list-style-type: none"> - Comparing the classification performance of the studied brain imaging data showed the following resulting order: FreeSurfer > VBM > FDG > Florbetapir. - Working with ROI values extracted from the temporal lobe, hippocampus, and amygdala showed that the atrophy of the regional brain occurs initially and most severely in the entorhinal cortex and hippocampus before spreading throughout the neocortex. 			
Dataset	ADNI				
Fused Modalities	MRI and (Florbetapir and FDG) PET				
Scanning Char.	-				
Brain Region	MRI: mean GM, mean CTH and volumetric measure <i>Note: mean GM extracted from VBM and mean CTH and volumetric measure extracted from FreeSurfer version 5.1.</i> Florbetapir-PET: brain amyloid β burden FDG-PET: glucose metabolism				
Subjects	Group	NC	MCI	AD	
	No.	98	Early MCI (E-MCI): 174	-	-
	Age	-	-	-	-
System Char.	Automatic/Objective				
Ref.	105				
Approach details	Goal	Classification (SAE (feature representation), multi-task learning (feature selection), MK-SVM learning (multi-modality fusion))			
	Notes	-			
	Type	Supervised			
	Results	<ul style="list-style-type: none"> - The proposed system with MK-SVM showed the best performance for AD vs. NC, MCI vs. NC, MCI-C vs. MCI-NC binary classification problems. These performance accuracies were 95.9%, 85.0%, and 75.8%, respectively. - Regarding MCI-C vs. MCI-NC, the system could improve the performance by 4.0% which is important for early diagnosis purposes. 			
	Clinical findings	Assisting the experts in the early diagnosis of AD.			
Dataset	ADNI				

Medical imaging diagnosis of early Alzheimer's disease

Fused Modalities	MRI, PET, and CSF <i>Note: MMSE and ADAS-Cog were also provided for each subject</i>				
Scanning Char.	-				
Brain Region	MRI: GM tissue volume from MRI and PET: the mean intensity CSF: $A\beta_{42}$, t -tau, and p -tau				
Subjects	Group	NC	MCI		AD
	No.	52	MCI-C	MCI-NC	51
			43	56	
Age	-	-	-	-	
System Char.	Automatic/Objective				

Ref.	106				
Approach details	Goal	Feature selection model (M2TFS)			
	Notes	<p>- The classification was performed as a multi-task learning process where each task focused on each modality's classification. To achieve that, SVM was used where for each modality, a linear kernel was first calculated using the obtained features. Then, MK-SVM was adopted for multi-modality classification combination.</p> <p>- Two regularization items were included: 1-Group Lasso regularizer: jointly selected a small number of features across different modalities. 2-Laplacian regularization term: the whole data related geometric distribution information was preserved from each modality.</p>			
	Type	-			
	Results	<p>- For the supervised classification task: The proposed M2TFS model achieved better accuracy and sensitivity results than compared methods. For accuracy, it achieved 95.03%, 79.27% and 68.94% for classification problems of AD vs. NC, MCI vs. NC, and MCI-C vs. MCI-NC, respectively.</p> <p>- For the semi-supervised classification task: The accuracy of the classification improved consistently with the increase of the unlabeled samples on the three groups of classification. These findings revealed that the proposed model could lead to the more discriminant feature selection using the geometric distribution of the data.</p>			
	Clinical findings	Assisting the experts in the early diagnosis of AD.			

Dataset	ADNI				
Fused Modalities	MRI, PET				
Scanning Char.	-				
Brain Region	MRI: GM PET: average intensity				
Subjects	Group	NC	MCI		AD
	No.	52	MCI-C	MCI-NC	51
			43	56	
Age	-	-	-	-	
System Char.	Automatic/Objective				

Ref.	107				
Approach details	Goal	Feature representation and multimodal data fusion (Deep Boltzman Machine).			
	Notes	Rather than dealing with the GM density values as in related literature, this study relied on the latent high-level feature representation and proposed a method of extracting a shared feature representation from MRI and PET by utilizing deep learning concept.			
	Type	Supervised			
	Results	Obtained the following maximal accuracies for binary classification problems: 95.3.5% for AD vs. NC, 85.6.7% for MCI vs. NC and 74.5.8% for MCI-C vs. MCI- NC			
	Clinical findings	The proposed method could discover the complex latent patterns hidden in MRI and PET in a hierarchical manner.			

Medical imaging diagnosis of early Alzheimer's disease

Dataset	ADNI				
Fused Modalities	MRI and FDG-PET				
Scanning Char.	<p>- The structural MR images were acquired from 1.5 T scanners. The data were downloaded in the neuroimaging informatics technology initiative (NIFTI) format, which had been pre-processed for the correction of the spatial distortion that occurred through both of the gradient nonlinearity and B1 field inhomogeneity.</p> <p>- The FDG-PET images were acquired 30–60 min post-injection, averaged, spatially aligned, interpolated to a standard voxel size, normalized in intensity, and smoothed to a common resolution of 8 mm full width at half maximum.</p>				
Brain Region	Latent high-level MRI and PET features.				
Subjects	Group	NC	MCI		AD
	No.	101	MCI-C	MCI-NC	93
			76	128	
	Age (range) (mean \pm SD)	(62–87) 75.9 \pm 4.8	(55–89) 75.0 \pm 7.2		(55–88) 75.5 \pm 7.4
System Char.	Automatic/Objective				

Ref.	109				
Approach details	Goal	Estimating multi-modality imaging data (3D CNN)			
	Notes	<p>- The study relied on volumetric modalities where one of them was used as an input (MRI) and the other as an output (PET). The goal was to capture the nonlinear relationship between the two modalities. The idea behind this procedure was to allow the prediction of the missing patterns of the PET from the images of the MR.</p>			
	Type	Supervised			
	Results	<p>- The tested data contains 398 subjects with both PET and MRI images. Therefore, the first test was to randomly use half of these images for training the 3D-CNN model followed by PET prediction using the remaining half. The evaluation showed the possibility of the proposed method to successfully estimate the PET images.</p> <p>- Two classification tests were performed. The first one tested the features obtained from the PET and MRI separately while the other one tested the features' combination. For the first test, the proposed method, in general, showed better results when compared with KNN and Zero methods even when the true PET images or the predicted ones were used. Also, the predicted results of PET were comparable with the true PET images. These results reflected the possibility of the proposed method to improve the diagnosis accuracy through its predicted PET. On the other hand, testing the combination of the PET and MRI features showed an improvement in the performance.</p>			
	Clinical findings	Assisting the experts in the early diagnosis of AD.			
Dataset	ADNI				
Fused Modalities	MRI and PET				
Scanning Char.	-				
Brain Region	MRI: GM tissue density maps				
Subjects	Group	NC	MCI		AD
	No.	229	MCI-C	MCI-NC	198
			167	236	
	Age (mean)	-	-	-	-
	Note:	of these subjects did not have corresponding PET images.			
System Char.	Automatic/Objective				

Ref.	108				
Approach details	Goal	Feature representation (SAE)			
	Notes	-			
	Type	Unsupervised			
	Results	<p>Obtained the following accuracies for binary classification problems:</p> <p>98.8% for AD vs. NC, 90.7% for MCI vs. NC 83.7% of AD vs. MCI and 83.3% of MCI-C vs. MCI- NC</p>			
	Clinical findings	The pre-training related unsupervision characteristic in deep learning helped in discovering general latent feature representations that consequently led to classification accuracy enhancement.			
Dataset	ADNI				

Medical imaging diagnosis of early Alzheimer's disease

Fused Modalities	MRI, FDG-PET and CSF data <i>Note: MMSE and ADAS-Cog were also provided for each patient.</i>				
Scanning Char.	<p>- The structural MR images were acquired from 1.5 T scanners. The data were downloaded in the NIfTI format, which had been pre-processed for the correction of the spatial distortion that occurred through both of the gradient nonlinearity and B1 field inhomogeneity.</p> <p>- The FDG-PET images were acquired 30–60 min post-injection, averaged, spatially aligned, interpolated to a standard voxel size, normalized in intensity, and smoothed to a common resolution of 8 mm full width at half maximum.</p> <p>- CSF data were collected in the morning after a fast for overnight by a needle of 20- or 24-gauge spinal that frozen within 1 collection hour, and transported on dry ice to the University of Pennsylvania Medical Center for the Laboratory of the ADNI Biomarker Core.</p>				
Brain Region	MRI: GM PET: mean intensity CSF: A β_{42} , t-tau, and p-tau				
Subjects	Group	NC	MCI		AD
	No.	52	MCI-C	MCI-NC	51
			43	56	
	Age (range) (mean \pm SD)	(62–85) 75.3 \pm 5.2	(58–88) 75.7 \pm 6.9	(55–89) 75.0 \pm 7.1	(59–88) 75.2 \pm 7.4
System Char.	Automatic/Objective				
Ref.	110				
Approach details	Goal	CAD system (sparse SAE (representation), softmax regression layer (classification))			
	Notes	-			
	Type	Semi-supervised			
	Results	<p>- Two binary classification problems were addressed (AD vs. NC and MCI vs. NC) where the proposed method achieved the better results than SK- and MK- SVM for the classification of AD vs. NC. For MCI vs. NC classification problem, MK-SVM showed better results immediately followed with an almost even accuracy of the proposed method.</p> <p>- Regarding sensitivity, the proposed system showed the higher accuracy than the SK- and MK-SVM in both of the classification problems. These results were useful since the higher sensitivity results benefited the diagnosis process.</p> <p>- Comparing the classification performance of each class separately (NC, MCI-C, MCI-NC, and AD). The experiments showed better accuracy results of the proposed method than SVM with regard to NC, MCI-NC, and AD. In MCI-C, MK-SVM achieved better results. Computing the overall accuracy showed better results of the proposed method than SVM.</p>			
	Clinical findings	Assisting the experts in the early diagnosis of AD.			
Dataset	ADNI				
Fused Modalities	MRI and PET				
Scanning Char.	-				
Brain Region	MRI: GM PET: cerebral metabolic rate of glucose consumption (CMRGlc)				
Subjects	Group	NC	MCI		AD
	No.	77	MCI-C	MCI-NC	65
			67	102	
	Age	-	-	-	-
System Char.	Automatic/Objective				
Ref.	112				
Approach details	Goal	Improving the neuroimaging biomarker identification quality of AD/MCI through presenting: 1) nonlinear feature transformation (thin-plate splines (TPS) metric learning (TML)-SVM) and 2) feature fusion (multi-modal stacked denoising sparse auto-encoder (DSAE))			
	Notes	-			
	Type	Supervised			
	Results	<p>The proposed work obtained better results from different comparisons' perspectives:</p> <p>1-Comparing the proposed combination of the extracted longitudinal and baseline features of the cases of using each of the extracted features individually.</p> <p>2-Comparing the proposed fusion strategy against other strategies.</p> <p>3-Comparing the proposed classifier against other state-of-the-art classifiers.</p>			
	Clinical findings	<p>- Fusing longitudinal and baseline feature serviced the classification target more than utilizing these features individually.</p> <p>- Improving the identification ability of the AD/MCI subjects against NC subjects.</p>			

Medical imaging diagnosis of early Alzheimer's disease

Dataset	ADNI			
Fused Modalities	Cross-sectional (GM tissue densities) and longitudinal (DM) features that estimated from the MRI			
Scanning Char.	-			
Brain Region	Structure of the brain <i>Note: focused on the cross-sectional and longitudinal features that estimated from the MRI.</i>			
Subjects	Group	NC	MCI	AD
	No.	123	121	94
	Age	-	-	-
System Char.	Automatic/Objective			

Ref.	113			
Approach details	Goal	Classification (PCA (feature extraction), stability selection technique, least absolute shrinkage and a selection operator (Lasso) method (feature selection), deep learning system (modeling weights), SVM (classification))		
	Notes	<ul style="list-style-type: none"> - Modeling the weights in the deep structure was made in two phases: initialization through unsupervised training then fine-tuning using the labels of AD patients by employing dropout technique. - The dropout technique was utilized to improve the generalization capability of the model. - SVM was used for AD/MCI classification using the learned features representation. - The deep learning structure was treated as multitasking learning framework. - The class label learning, MMSE, and ADAS-Cog were treated as related tasks to improve the class label prediction. - The authors incorporated the stability selection technique (an adaptive learning factor) and multitask learning strategy in the proposed deep learning framework. 		
	Type	Supervised		
	Results	<ul style="list-style-type: none"> - The best performance of the system was 91.4% in diagnosing AD, 77.4% in diagnosing MCI and 70.1% in diagnosing AD vs. MCI. - In the diagnosis of MCI-C vs. MCI-NC, the PCA found to degrade the results slightly from 58.1% to 57.4%. - The dropout technique helped in improving the classification accuracy than the classical deep learning methods by 5.9%. - Identifying the impact of each of the model components showed that the largest impact was through dropout component, followed by multitasking learning, then stability selection technique and ending with PCA. - The performance of deep model without dropout was comparable with the baseline method (feature selection +SVM). - The authors suggested that the deep traditional learning could not extract information efficiently from datasets with small size unless a regularization technique such as dropout is used. 		
	Clinical findings	Assisting the experts in the early diagnosis of AD.		

Dataset	ADNI				
Fused Modalities	MRI, PET, and CSF				
Scanning Char.	-				
Brain Region	MRI and PET: volumetric features CSF: β_{42} , t -tau, and p -tau				
Subjects	Group	NC	MCI		AD
	No.	52	MCI-C	MCI-NC	51
			43	56	
	Age	-	-	-	-
	Note:	Two additional clinical scores for each patient were also used: MMSE and ADAS-Cog			
System Char.	Automatic/Objective				

Ref.	111			
Approach details	Goal	Classification (SAE and a softmax logistic regressor)		
	Notes	<ul style="list-style-type: none"> - Unsupervised feature representation was embedded in the framework. - For data fusion: the proposed framework utilized a zero-masking strategy to fuse complementary information that obtained from multiple modalities. 		
	Type	Supervised		
	Results	The proposed framework obtained better results than SVM and other deep learning frameworks.		
	Clinical findings	The system showed performance gain in both the binary as well as the multiclass classification tasks of the disease.		

Medical imaging diagnosis of early Alzheimer's disease

Dataset	ADNI					
Fused Modalities	MRI and FDG-PET					
Scanning Char.	-					
Brain Region	MRI: Structure of the brain PET: Function of the brain					
Subjects	For unimodal dataset (only MRI)	Group	NC	MCI		AD
		No.	204	MCI-C	MCI-NC	180
				160	214	
	Age	-	-	-	-	
	For multimodal dataset (MRI & PET)	Group	NC	MCI		AD
		No.	77	MCI-C	MCI-NC	85
			67	102		
Age	-	-	-	-		
System Char.	Automatic/Objective					

Ref.	114				
Approach details	Goal	Prediction model (ELMs (prediction))			
	Notes	-			
	Type	Supervised			
	Results	<p>- To evaluate the complimentary of the each of the three biomarkers, the study evaluated MRI based-ELM, PET based-ELM, CSF based-ELM and combined information based-ELM. Regarding single biomarkers, the MRI and CSF-based prediction capabilities showed close results with higher MRI-based sensitivity more slightly than CSF. For PET it showed the lowest results, but this did not prevent it from being used to differentiate MCI from NC as its correlation coefficient could achieve 0.2086.</p> <p>- The proposed model achieved the best accuracy with the combination of the three biomarkers that indicated the complimentary of them when differentiating MCI from NC.</p> <p>- Comparing the proposed combined based ELM model against SVM and SVM-fusion showed the better accuracy of the proposed model but slightly lower sensitivity than SVM.</p>			
	Clinical findings	Assisting the experts in the early diagnosis of AD.			
Dataset	ADNI				
Fused Modalities	MRI, PET, and CSF				
Scanning Char.	-				
Brain Region	Structural and functional information.				
Subjects	Group	NC	MCI		AD
	No.	52	MCI-C	MCI-NC	-
			43	56	
	Age	-	-	-	-
System Char.	Automatic/Objective				

Ref.	115				
Approach details	Goal	Classification of MCI-C and MCI-NC (M2TL (sample selection and classification))			
	Notes	<p>- The study utilized samples from different domains (i.e. AD/NC) in a transfer learning manner to help in the discrimination task of MCI-C and MCI-NC.</p> <p>- Due to the distributions differences of the auxiliary and target domains, the study utilized MMD criterion as a similarity/dissimilarity measure between two samples from different domains.</p> <p>- To reflect the relation among the samples of the target domain, the auxiliary domain, and the unlabeled samples, the study designed a cross-domain Laplacian matrix.</p> <p>- Finally, in the objective function, a group sparsity constraint was used to help in the informative sample selection to predict the labels of the target class.</p>			
	Type	-			
	Results	The proposed method showed consistent and substantial improvement in the prediction accuracy of the MCI conversion, where the maximum accuracy achieved 80.1%.			
	Clinical findings	Assisting the experts in the early diagnosis of AD.			

Medical imaging diagnosis of early Alzheimer's disease

Dataset	ADNI				
Fused Modalities	MRI, PET, and CSF				
Scanning Char.	MRI: were acquired from 1.5.T scanners. PET: were acquired 30–60 min post-injection. CSF: were collected in the morning after a fast for overnight by a needle of 20- or 24-gauge spinal, frozen within 1 collection hour, and transported on dry ice to the University of Pennsylvania Medical Center for the ADNI Biomarker Core laboratory.				
Brain Region	MRI: GM tissue volume PET: average intensity CSF: $A\beta_{42}$, t -tau, and p -tau.				
Subjects	Group	NC	MCI		AD
	No.	52	MCI-C	MCI-NC	51
			43	56	
	Age	-	-	-	-
System Char.	Automatic/Objective				
Ref.	116				
Approach details	Goal	Classification of MCI-C and MCI-NC (transfer learning and multi-label learning (feature selection), MK-SVM (classification), MK relevance vector regression machine (regression))			
	Notes	Based on transfer learning and multi-label learning, the study proposed MDML method for selecting the most informative features from multi-domain data.			
	Type	Supervised			
	Results	<ul style="list-style-type: none"> - The proposed MDML showed better classification results of MCI-C vs. MCI-NC than the compared methods when testing the performance on different modalities (MRI, PET, MRI+PET+CSF). The method achieved accuracies of 73.2%, 70.0%, and 78.7%, respectively. - Additionally, the study tested the prediction of the clinical scores (i.e. MMSE/ADAS-Cog) using different modalities (MRI, PET, MRI+PET+CSF). The tests showed better prediction results than the compared methods. Noteworthy, the proposed MDML method accomplished the prediction task without related learning domain. 			
	Clinical findings	The method could successfully found out the most discriminant regions of the brain (e.g. hippocampal, amygdala, temporal lobe, precuneus, and insula).			
Dataset	ADNI				
Fused Modalities	MRI, PET, CSF, MMSE, and ADAS-Cog data				
Scanning Char.	MRI: were acquired from 1.5.T scanners. PET: were acquired 30–60 min post-injection. CSF: were collected in the morning after a fast for overnight by a needle of 20- or 24-gauge spinal, frozen within 1 collection hour, and transported on dry ice to the University of Pennsylvania Medical Center for the ADNI Biomarker Core laboratory.				
Brain Region	MRI: GM tissue volume PET: average intensity CSF: $A\beta_{42}$, t -tau, and p -tau.				
Subjects	Group	NC	MCI		AD
	No.	52	MCI-C	MCI-NC	51
			43	56	
	Age	-	-	-	-
	Note	AD and NC data were used as learning domain while MCI were used as target domain.			
System Char.	Automatic/Objective				

Dependency upon the enrolled data also represents a source of limitations in the context of applying computerized methods/techniques with AD. In other words, some implementations require adaptation of certain parameters depending on the case studies that prevent such results from being generalized unless otherwise verifying its performance. Therefore, in general, further advances are still needed to help enhance the quality of the

applied methods/techniques to achieve maximum benefits in their implementation.

4.4. Subjects

The subjects themselves also represent another obstacle for further development in the context of AD. For example, the movement of patients during the image acquisition process introduces a source of the

noise. It can be detected either by preprocessing steps or by taking such movements into consideration during further work (e.g., slow eye movement during the earliest phase of drowsiness when recording EEG signals).

In addition, comorbidities can lead to misclassification. In other words, it prevents accurate decision making regarding the stage of the AD due to the overlap that may occur between the disorders' symptoms. Furthermore, patients may have counter-indications for or present with medical treatments which prevent the use of some diagnostic equipment or modalities (e.g., implanted metallic devices which prevent the use of MRI).

5. CONCLUSION

AD is the most common neurodegenerative disease affecting the CNS. AD patients experience several stages during their disease journey. Among these stages, the early stage is the most difficult stage to diagnose due to multiple factors, mainly because pathological symptoms begin nearly ten to fifteen years before clinical diagnosis. Numerous research efforts target this stage of AD hoping to reveal as much information as possible to assist the early diagnosis of AD. The aim of this paper is to monitor the current efforts in this area. The findings of this paper are presented from two perspectives, computer-based as well as clinical findings. As illustrated, the main scanning technologies that presently serve this area are MRI, PET, and SPECT technologies. Along with the use of these technologies individually, fusing different features of a single technology in addition to fusing different technologies show promising results. The cumulative information obtained from these technologies may consequently assist the diagnosis process. Despite the current advances, the door is still open to further efforts. The rapid progress in the scanning technologies, computer-based techniques, and the databases repositories represent the main factors that encourage researchers to continue work in this research area.

6. ACKNOWLEDGEMENTS

Ayman S. El-Baz and Hassan Hajjdiab are sharing the senior authorship.

7. REFERENCES

1. "World Health Organization," <http://www.who.int/>
2. J. Hodler, G. von Schulthess, and C. Zollikofer (Eds): Diseases of the Brain, Head & Neck, Spine 2012–2015. *Springer*, Milan, (2012)
DOI: 10.1007/978-88-470-2628-5
3. D. Brown (Ed): Brain Diseases and Metalloproteins. *Pan Stanford Pub.*, Singapore (2013)
4. S. Gauthier (Ed): Clinical Diagnosis and Management of Alzheimer's Disease. *CRC Press* (2006)
DOI: 10.3109/9780203931714
5. L. Lu, and J. Bludau: Alzheimer's Disease (Biographies of Disease). *Greenwood Publishing Group* (2011)
6. L. Scinto, and K. Daffner (Eds): Early Diagnosis of Alzheimer's Disease. *Humana Press*, Totowa, NJ (2000)
DOI: 10.1385/1592590055
7. C. Turkington, and J. Harris: The Encyclopedia of the Brain and Brain Disorders. *Infobase Publishing* (2010)
8. A. Osborn, K. Salzman, M. Jhaveri, and A. Barkovich: Diagnostic Imaging: Brain. *Elsevier Health Sciences* (2015)
9. S. Chamberlin, and B. Narins (Eds): The Gale Encyclopedia of Neurological Disorders. *Thomson Gale* (2005)
10. C. Starkey: Therapeutic Modalities. *F. A. Davis Co* (2013)
11. <http://www.alzheimer-research.eu>
12. <http://www.nia.nih.gov>
13. N. Ali: Understanding Alzheimer's: An Introduction for Patients and Caregivers. *Rowman & Littlefield Publishers*, Lanham, MD (2012)
14. N. Smith, and A. Webb: Introduction to Medical Imaging. *Cambridge University Press*, Cambridge (2011)
15. R. Chaves, J. Ramírez, and J. Górriz: Integrating discretization and association rule-based classification for Alzheimer's disease diagnosis. *Expert Syst Appl*40, 1571–1578 (2013)
DOI: 10.1016/j.eswa.2012.09.003
16. S. Belleville, C. Fouquet, S. Duchesne, D. Collins, and C. Hudon: Detecting early preclinical Alzheimer's disease via cognition, neuropsychiatry, and neuroimaging: qualitative review and recommendations for testing. *J Alzheimers Dis*42, S375-S382 (2014)

17. K. Blennow, B. Dubois, A. Fagan, P. Lewczuk, M. de Leon, and H. Hampel: Clinical utility of cerebrospinal fluid biomarkers in the diagnosis of early Alzheimer's disease. *Alzheimers Dement*11, 58–69 (2015)
DOI: 10.1016/j.jalz.2014.02.004
18. G. Chételat, R. La Joie, N. Villain, A. Perrotin, V. de La Sayette, F. Eustache, and R. Vandenberghe: Amyloid imaging in cognitively normal individuals, at-risk populations and preclinical Alzheimer's disease. *Neuroimage Clin*2, 356–365 (2013)
DOI: 10.1016/j.nicl.2013.02.006
19. A. Cohen, and W. Klunk: Early detection of Alzheimer's disease using PiB and FDG PET. *Neurobiol Dis*72, 117–122 (2014)
DOI: 10.1016/j.nbd.2014.05.001
20. M. Ewers, R. Sperling, W. Klunk, M. Weiner, and H. Hampel: Neuroimaging markers for the prediction and early diagnosis of Alzheimer's disease dementia. *Trends Neurosci*34, 430–442 (2011)
DOI: 10.1016/j.tins.2011.05.005
21. O. Forlenza, B. Diniz, A. Teixeira, F. Stella, and W. Gattaz: Mild cognitive impairment (part 2): biological markers for diagnosis and prediction of dementia in Alzheimer's disease. *Rev Bras Psiquiatr*35, 284–294 (2013)
DOI: 10.1590/1516-4446-2012-3505
22. E. Reiman, and W. Jagust: Brain imaging in the study of Alzheimer's disease. *Neuroimage*61, 505–516 (2012)
DOI: 10.1016/j.neuroimage.2011.11.075
23. S. Risacher, and A. Saykin: Neuroimaging and other biomarkers for Alzheimer's disease: The changing landscape of early detection. *Annu Rev Clin Psycho*9, 621–648 (2013)
DOI: 10.1146/annurev-clinpsy-050212-185535
24. R. Sperling, B. Dickerson, M. Pihlajamaki, P. Vannini, P. LaViolette, O. Vitolo, T. Hedden, J. Becker, D. Rentz, D. Selkoe, and K. Johnson: Functional alterations in memory networks in early Alzheimer's disease. *Neuromol Med*12, 27–43 (2010)
DOI: 10.1007/s12017-009-8109-7
25. S. Tumati, S. Martens, and A. Aleman: Magnetic resonance spectroscopy in mild cognitive impairment: systematic review and meta-analysis. *Neurosci Biobehav Rev*37, 2571–2586 (2013)
DOI: 10.1016/j.neubiorev.2013.08.004
26. T. Varghese, R. Sheelakumari, J. James, and P. Mathuranath: A review of neuroimaging biomarkers of Alzheimer's disease. *Neurol Asia*18, 239–248 (2013)
27. A. Vlassenko, T. Benzinger, and J. Morris: PET amyloid-beta imaging in preclinical Alzheimer's disease. *BBA-Mol Basis Dis*1822, 370–379 (2012)
DOI: 10.1016/j.bbadis.2011.11.005
28. T. Farncombe, and K. Iniewski (Eds): Medical Imaging. *CRC Press/Taylor & Francis Group*, Boca Raton, FL (2013)
29. M. Haidekker: Medical Imaging Technology. *Springer*, New York (2013)
DOI: 10.1007/978-1-4614-7073-1
30. S. Eskildsen, P. Coupé, V. Fonov, J. Pruessner, and D. Collins: Structural imaging biomarkers of Alzheimer's disease: predicting disease progression. *Neurobiol Aging*36, S23-S31 (2015)
DOI: 10.1016/j.neurobiolaging.2014.04.034
31. K. Nayaki, and A. Varghese: Alzheimer's detection at early stage using local measures on MRI: a comparative study on local measures. *2014 International Conference on Data Science & Engineering (ICDSE)*, August 26–28, Kochi, India, 224–227 (2014)
32. C. Salvatore, A. Cerasa, P. Battista, M. Gilardi, A. Quattrone, and I. Castiglioni: Magnetic resonance imaging biomarkers for the early diagnosis of Alzheimer's disease: a machine learning approach. *Front Neurosci*9, 307 (2015)
33. S. Lehericy, M. Baulac, J. Chiras, L. Piérot, N. Martin, B. Pillon, B. Deweer, B. Dubois, and C. Marsault: Amygdalohippocampal MR volume measurements in the early stages of Alzheimer disease. *Am J Neuroradiol*15, 929–937 (1994)
34. C. Dennis, C. Nick, I. Rachael, R. William, L. Jennifer, L. Guy, M. Alex, M. John, C. Lisa, and N. Martin: Patterns of temporal lobe atrophy in semantic dementia and Alzheimer's disease. *Ann Neurol*49, 433–442 (2001)
DOI: 10.1002/ana.92

35. B. Dickerson, I. Goncharova, M. Sullivan, C. Forchetti, R. Wilson, D. Bennett, L. Beckett, and L. deToledo-Morrell: MRI-derived entorhinal and hippocampal atrophy in incipient and very mild Alzheimer's disease. *Neurobiol Aging*22, 747–754 (2001)
DOI: 10.1016/S0197-4580(01)00271-8
36. R. Killiany, B. Hyman, T. Gomez-Isla, M. Moss, R. Kikinis, F. Jolesz, R. Tanzi, K. Jones, and M. Albert: MRI measures of entorhinal cortex vs hippocampus in preclinical AD. *Neurology*58, 1188–1196 (2002)
DOI: 10.1212/WNL.58.8.1188
37. S. Yang, J. Lee, C. Huang, J. Wang, W. Hsu, and Y. Wai: An image-aided diagnosis system for dementia classification based on multiple features and self-organizing map. In: Neural Information Processing. Models and Applications. ICONIP 2010. Lecture Notes in Computer Science, 6444. Eds: KW Wong, BS Mendis, A Bouzerdoum Springer, Berlin, Heidelberg, 462–469 (2010)
DOI: 10.1007/978-3-642-17534-3_57
38. J. Pa, A. Boxer, L. Chao, A. Gazzaley, K. Freeman, J. Kramer, B. Miller, M. Weiner, J. Neuhaus, and J. Johnson: Clinical-neuroimaging characteristics of dysexecutive mild cognitive impairment. *Ann Neurol*65, 414–423 (2009)
DOI: 10.1002/ana.21591
39. R. Wolz, V. Julkunen, J. Koikkalainen, E. Niskanen, D. Zhang, D. Rueckert, H. Soininen, and J. Lötjönen: Multi-method analysis of MRI images in early diagnostics of Alzheimer's disease. *PLoS ONE*6, e25446 (2011)
DOI: 10.1371/journal.pone.0025446
40. T. Varghese, R. Kumari, P. Mathuranath, and N. Albert Singh: Performance evaluation of bacterial foraging optimization algorithm for the early diagnosis and tracking of Alzheimer's disease. In: Swarm, Evolutionary, and Memetic Computing. SEMCCO 2012. Lecture Notes in Computer Science, 7677. Eds: BK Panigrahi, S Das, PN Suganthan, PK Nanda Springer, Berlin, Heidelberg, 41–48 (2012)
41. R. Mahmood, and B. Ghimire: Automatic detection and classification of Alzheimer's Disease from MRI scans using principal component analysis and artificial neural networks. In: 2013 20th International Conference on Systems, Signals and Image Processing (IWSSIP), 7–9 July, Bucharest, Romania, 133–137 (2013)
42. Y. Shi, X. Zhang, and Z. Liu: Automatic segmentation of hippocampal subfields based on multi-atlas image segmentation techniques. *J Electron(China)*31, 121–128 (2014)
DOI: 10.1007/s11767-014-3183-x
43. P. Mondal, J. Mukhopadhyay, S. Sural, and P. Bhattacharyya: 3D-SIFT feature based brain atlas generation: An application to early diagnosis of Alzheimer's disease. 2014 International Conference on Medical Imaging, m-Health and Emerging Communication Systems (MedCom), 7–8 November, Noida, India, 342–347 (2014)
44. D. López-Rodríguez, and A. García-Linares: Predictive and populational model for Alzheimer's disease using structural neuroimaging. In: XIII Mediterranean Conference on Medical and Biological Engineering and Computing 2013. IFMBE Proceedings, 41, IFMBE Proceedings, 41. Eds: Roa Romero L Springer, Cham, 285–288 (2014)
DOI: 10.1007/978-3-319-00846-2_71
45. A. Payan, and G. Montana: Predicting Alzheimer's disease: a neuroimaging study with 3D convolutional neural networks. *arXiv preprint arXiv:1502.0.2506*, (2015)
46. L. Khedher, J. Ramírez, J. Górriz, A. Brahim, and F. Segovia: Early diagnosis of Alzheimer's disease based on partial least squares, principal component analysis and support vector machine using segmented MRI images. *Neurocomputing*151, 139–150 (2015)
DOI: 10.1016/j.neucom.2014.09.072
47. L. Khedher, J. Ramírez, J. Górriz, A. Brahim, and I. Illán: Independent component analysis-based classification of Alzheimer's disease from segmented MRI data. In: Artificial Computation in Biology and Medicine. IWINAC 2015. Lecture Notes Computer Science, 9107, Springer, Cham, 78–87 (2015)
DOI: 10.1007/978-3-319-18914-7_9
48. E. Hosseini-Asl, G. Gimel'farb, and A. El-Baz: Alzheimer's Disease Diagnostics by a Deeply Supervised Adaptable 3D Convolutional Network. *arXiv preprint arXiv:1607.0.0556*, (2016)

49. E. Hosseini-Asl, R. Keynton, and A. El-Baz: Alzheimer's disease diagnostics by adaptation of 3D convolutional network. In: 2016 IEEE International Conference on Image Processing (ICIP), 126–130 (2016)
50. M. Liu, D. Zhang, E. Adeli, and D. Shen: Inherent structure-based multiview learning with multitemplate feature representation for Alzheimer's disease diagnosis. *IEEE Trans Biomed Eng*63, 1473–1482 (2016)
DOI: 10.1109/TBME.2015.2496233
51. G. Maicas, A. Muñoz, G. Galiano, A. Hamza, and E. Schiavi: Spectral shape analysis of the hippocampal structure for Alzheimer's disease diagnosis. *SEMA SIMAI Springer Series*8, 17–32 (2016)
DOI: 10.1007/978-3-319-32013-7_2
52. F. El-Gamal, M. Elmogy, and A. Atwan: Current trends in medical image registration and fusion. *Egypt Inform J*17, 99–124 (2016)
DOI: 10.1016/j.eij.2015.09.002
53. D. Kogure, H. Matsuda, T. Ohnishi, T. Asada, M. Uno, T. Kunihiro, S. Nakano, and M. Takasaki: Longitudinal evaluation of early Alzheimer's disease using brain perfusion SPECT. *J Nucl Med*41, 1155–1162 (2000)
54. K. Ishii, F. Willoch, S. Minoshima, A. Drzezga, E. Ficaró, D. Cross, D. Kuhl, and M. Schwaiger: Statistical brain mapping of ¹⁸F-FDG PET in Alzheimer's disease: validation of anatomic standardization for atrophied brains. *J Nucl Med*42, 548–557 (2001)
55. G. Alexander, K. Chen, P. Pietrini, S. Rapoport, and E. Reiman: Longitudinal PET evaluation of cerebral metabolic decline in dementia: a potential outcome measure in Alzheimer's disease treatment studies. *Am J Psychiatry*159, 738–745 (2002)
DOI: 10.1176/appi.ajp.159.5.738
56. K. Bradley, V. O'Sullivan, N. Soper, Z. Nagy, E. King, A. Smith, and B. Shepstone: Cerebral perfusion SPET correlated with Braak pathological stage in Alzheimer's disease. *Brain*125, 1772–1781 (2002)
DOI: 10.1093/brain/awf185
57. A. Elgazzar (Ed): The Pathophysiologic Basis of Nuclear Medicine. *Springer-Verlag Berlin Heidelberg*, Berlin, Heidelberg (2006)
DOI: 10.1007/978-3-540-47953-6
58. R. Van Heertum, R. Tikofsky, and M. Ichise (Eds): Functional cerebral SPECT and PET imaging. *Wolters Kluwer/Lippincott Williams & Wilkins*, Philadelphia, PA (2010)
59. J. Jiménez Bonilla, and J. Carril Carril: Molecular neuroimaging in degenerative dementias. *Rev Esp Med Nucl Imagen Mol* 32, 301–309 (2013)
DOI: 10.1016/j.remnie.2013.07.027
60. R. Sperling, P. Aisen, L. Beckett, D. Bennett, S. Craft, A. Fagan, T. Iwatsubo, C. Jack, J. Kaye, T. Montine, D. Park, E. Reiman, C. Rowe, E. Siemers, Y. Stern, K. Yaffe, M. Carrillo, B. Thies, M. Morrison-Bogorad, M. Wagster, and C. Phelps: Toward defining the preclinical stages of Alzheimer's disease: Recommendations from the National Institute on Aging-Alzheimer's Association workgroups on diagnostic guidelines for Alzheimer's disease. *Alzheimer's & Dementia*7, 280–292 (2011)
DOI: 10.1016/j.jalz.2011.03.003
61. D. Wolk, J. Price, J. Saxton, B. Snitz, J. James, O. Lopez, H. Aizenstein, A. Cohen, L. Weissfeld, C. Mathis, W. Klunk, and S. DeKosky: Amyloid imaging in mild cognitive impairment subtypes. *Ann Neurol*65, 557–568 (2009)
DOI: 10.1002/ana.21598
62. K. Pike, G. Savage, V. Villemagne, S. Ng, S. Moss, P. Maruff, C. Mathis, W. Klunk, C. Masters, and C. Rowe: Beta-amyloid imaging and memory in non-demented individuals: evidence for preclinical Alzheimer's disease. *Brain*130, 2837–2844 (2007)
DOI: 10.1093/brain/awm238
63. M. Ikonovic, W. Klunk, E. Abrahamson, C. Mathis, J. Price, N. Tsopelas, B. Lopresti, S. Ziolkó, W. Bi, W. Paljug, M. Debnath, C. Hope, B. Isanski, R. Hamilton, and S. DeKosky: Post-mortem correlates of in vivo PiB-PET amyloid imaging in a typical case of Alzheimer's disease. *Brain*131, 1630–1645 (2008)
DOI: 10.1093/brain/awn016
64. G. Chételat, B. Desgranges, V. de la Sayette, F. Viader, F. Eustache and J. Baron: Mild cognitive impairment: Can FDG-PET predict who is to rapidly convert to Alzheimer's disease? *Neurology*60, 1374–1377 (2003)
DOI: 10.1212/01.WNL.0000055847.17752.E6

65. D. Anchisi, B. Borroni, M. Franceschi, N. Kerrouche, E. Kalbe, B. Beuthien-Beumann, S. Cappa, O. Lenz, S. Ludecke, A. Marcone, R. Mielke, P. Ortelli, A. Padovani, O. Pelati, A. Pupi, E. Scarpini, S. Weisenbach, K. Herholz, E. Salmon, V. Holthoff, S. Sorbi, F. Fazio, and D. Perani: Heterogeneity of brain glucose metabolism in mild cognitive impairment and clinical progression to Alzheimer disease. *Arch Neurol*62, 1728–1733 (2005)
DOI: 10.1001/archneur.62.11.1728
66. A. Drzezga, T. Grimmer, M. Riemenschneider, N. Lautenschlager, H. Siebner, P. Alexopoulos, S. Minoshima, M. Schwaiger, and A. Kurz: Prediction of individual clinical outcome in MCI by means of genetic assessment and (¹⁸F)-FDG PET. *J Nucl Med* 46, 1625–1632 (2005)
67. I. Illan, J. Górriz, J. Ramírez, R. Chaves, F. Segovia, M. López, D. Salas-Gonzalez, P. Padilla, and C. Puntonet: Machine learning for very early Alzheimer's Disease diagnosis; a ¹⁸F-FDG and PiB PET comparison. In: Nuclear Science Symposium & Medical Imaging Conference, IEEE, Knoxville, TN, 2334–2337 (2010)
68. I. Illán, J. Górriz, J. Ramírez, D. Salas-Gonzalez, M. López, F. Segovia, R. Chaves, M. Gómez-Río, and C. Puntonet: ¹⁸F-FDG PET imaging analysis for computer aided Alzheimer's diagnosis. *Inform Sci*181, 903–916 (2011)
DOI: 10.1016/j.ins.2010.10.027
69. M. López, J. Ramírez, J. Górriz, I. Álvarez, D. Salas-Gonzalez, F. Segovia, R. Chaves, P. Padilla, and M. Gómez-Río: Principal component analysis-based techniques and supervised classification schemes for the early detection of Alzheimer's disease. *Neurocomputing*74, 1260–1271 (2011)
DOI: 10.1016/j.neucom.2010.06.025
70. F. Martínez-Murcia, J. Górriz, J. Ramírez, C. Puntonet, and D. Salas-González: Computer Aided Diagnosis tool for Alzheimer's Disease based on Mann-Whitney-Wilcoxon U-Test. *Expert Syst Appl* 9, 9676–9685 (2012)
DOI: 10.1016/j.eswa.2012.02.153
71. R. Chaves, J. Ramírez, J. Górriz, and I. Illán: Functional brain image classification using association rules defined over discriminant regions. *Pattern Recogn Lett*33, 1666–1672 (2012)
DOI: 10.1016/j.patrec.2012.04.011
72. R. Chaves, J. Ramírez, J. Górriz, and C. Puntonet: Association rule-based feature selection method for Alzheimer's disease diagnosis. *Expert Syst Appl*39, 11766–11774 (2012)
DOI: 10.1016/j.eswa.2012.04.075
73. P. Padilla, M. Lopez, J. M. Górriz, J. Ramirez, D. Salas-Gonzalez, and I. Alvarez: NMF-SVM based CAD tool applied to functional brain images for the diagnosis of Alzheimer's disease. *IEEE Trans Med Imaging*31, 207–216 (2012)
DOI: 10.1109/TMI.2011.2167628
74. P. Toussaint, V. Perlberg, P. Bellec, S. Desarnaud, L. Lacomblez, J. Doyon, M. Habert and H. Benali: Resting state FDG-PET functional connectivity as an early biomarker of Alzheimer's disease using conjoint univariate and independent component analyses. *Neuroimage*63, 936–946 (2012)
DOI: 10.1016/j.neuroimage.2012.03.091
75. S. Morbelli, A. Drzezga, R. Perneczky, G. Frisoni, A. Caroli, B. van Berckel, R. Ossenkoppele, E. Guedj, M. Didic, A. Brugnolo, G. Sambuceti, M. Pagani, E. Salmon, and F. Nobili: Resting metabolic connectivity in prodromal Alzheimer's disease. A European Alzheimer Disease Consortium (EADC) project. *Neurobiol Aging*33, 2533–2550 (2012)
DOI: 10.1016/j.neurobiolaging.2012.01.005
76. M. Ayhan, R. Benton, V. Raghavan, and S. Choubey: Composite kernels for automatic relevance determination in computerized diagnosis of Alzheimer's disease. In: Brain and Health Informatics. BHI 2013. Lecture Notes in Computer Science, 8211. Eds: K Imamura, S Usui, T Shirao, T Kasamatsu, L Schwabe, N Zhong Springer, Cham, 126–137 (2013)
DOI: 10.1007/978-3-319-02753-1_13
77. H. Aidos, J. Duarte, and A. Fred: Identifying regions of interest for discriminating Alzheimer's disease from mild cognitive impairment. In: 2014 IEEE International Conference on Image Processing (ICIP), 27–30 October, Paris, France (2014)
78. M. Bilgel, B. Jedynek, D. F. Wong, S. M. Resnick, and J. L. Prince: Temporal

- trajectory and progression score estimation from voxelwise longitudinal imaging measures: application to amyloid imaging. In: *Information Processing in Medical Imaging. Lecture Notes Computer Science*, 9123 , 424–436 (2015)
79. P. Padilla, J. Górriz, J. Ramírez, R. Chaves, F. Segovia, I. Alvarez, D. Salas-González, M. López, and C. Puntonet: Alzheimer's disease detection in functional images using 2D Gabor wavelet analysis. *Electron Lett*46, 556–558 (2010)
DOI: 10.1049/el.2010.0219
 80. P. Padilla, J. Górriz, J. Ramírez, E. Lang, R. Chaves, F. Segovia, M. López, D. Salas-González, and I. Álvarez: Analysis of SPECT brain images for the diagnosis of Alzheimer's disease based on NMF for feature extraction. *Neurosci Lett*479, 192–196 (2010)
DOI: 10.1016/j.neulet.2010.05.047
 81. P. Padilla, J. Górriz, J. Ramírez, E. Lang, R. Chaves, F. Segovia, I. Álvarez, D. Salas-González, and M. López: NMF-based analysis of SPECT brain images for the diagnosis of Alzheimer's disease. In: *Hybrid Artificial Intelligence Systems. HAIS 2010. Lecture Notes in Computer Science*, 6076. Eds: M Graña Romay, E Corchado, MT Garcia Sebastian Springer, Berlin, Heidelberg, 468–475 (2010)
DOI: 10.1007/978-3-642-13769-3_57
 82. J. Ramírez, J. Górriz, F. Segovia, R. Chaves, D. Salas-Gonzalez, M. López, I. Álvarez, and P. Padilla: Computer aided diagnosis system for the Alzheimer's disease based on partial least squares and random forest SPECT image classification. *Neurosci Lett*472, 99–103 (2010)
DOI: 10.1016/j.neulet.2010.01.056
 83. D. Salas-Gonzalez, J. Górriz, J. Ramírez, M. López, I. Álvarez, F. Segovia, R. Chaves, and C. Puntonet: Computer aided diagnosis of Alzheimer disease using support vector machines and classification trees. *Phys Med Biol*55, 2807–2817 (2010)
DOI: 10.1007/978-3-642-03040-6_51
 84. R. Chaves, J. Ramírez, J. Górriz, M. López, D. Salas-Gonzalez, I. Illán, F. Segovia, and P. Padilla: Effective Diagnosis of Alzheimer's disease by means of association rules. In: *Hybrid Artificial Intelligence Systems. HAIS 2010. Lecture Notes in Computer Science*, 6076. Eds: M Graña Romay, E Corchado, MT Garcia Sebastian Springer, Berlin, Heidelberg, 452–459 (2010)
DOI: 10.1007/978-3-642-13769-3_55
 85. R. Chaves, J. Ramírez, J. Górriz, D. Salas-Gonzalez, M. López, I. Illán, F. Segovia, and A. Olivares: Effective Diagnosis of Alzheimer's Disease by Means of Distance Metric Learning. In: *Hybrid Artificial Intelligent Systems. HAIS 2011. Lecture Notes in Computer Science*, 6678. Eds: E Corchado, M Kurzyński, M Woźniak Springer, Berlin, Heidelberg, 148–155 (2011)
DOI: 10.1007/978-3-642-21219-2_20
 86. I. Illán, J. Górriz, J. Ramírez, D. Salas-Gonzalez, M. López, F. Segovia, P. Padilla, and C. Puntonet: Projecting independent components of SPECT images for computer aided diagnosis of Alzheimer's disease. *Pattern Recogn Lett*31, 1342–1347 (2010)
DOI: 10.1016/j.patrec.2010.03.004
 87. I. Illán, J. Górriz, M. López, J. Ramírez, D. Salas-Gonzalez, F. Segovia, R. Chaves, and C. Puntonet: Computer aided diagnosis of Alzheimer's disease using component based SVM. *Appl Softw Comput*11, 2376–2382 (2011)
DOI: 10.1016/j.asoc.2010.08.019
 88. I. Illán, J. Górriz, J. Ramírez, E. Lang, D. Salas-Gonzalez and C. Puntonet: Bilateral symmetry aspects in computer-aided Alzheimer's disease diagnosis by single-photon emission-computed tomography imaging. *Artif Intell Med* 56, 191–198 (2012)
DOI: 10.1016/j.artmed.2012.09.005
 89. F. Martínez, D. Salas-González, J. Górriz, J. Ramírez, C. Puntonet, and M. Gómez-Río: Analysis of spect brain images using Wilcoxon and relative entropy criteria and quadratic multivariate classifiers for the diagnosis of Alzheimer's disease. In: *New Challenges on Bioinspired Applications. IWINAC 2011. Lecture Notes in Computer Science*, 6687. Eds: JM Ferrández, JR Álvarez Sánchez , F de la Paz, FJ Toledo Springer, Berlin, Heidelberg, 41–48 (2011)
DOI: 10.1007/978-3-642-21326-7_5
 90. F. Segovia, J. Górriz, J. Ramírez, D. Salas-González, and I. Álvarez: Early diagnosis of Alzheimer's disease based on partial least squares and support vector machine. *Expert Syst Appl*40, 677–683 (2013)
DOI: 10.1016/j.eswa.2012.07.071

91. M. Analoui, J. Bronzino, and D. Peterson (Eds): Medical Imaging: Principles and Practices. *CRC Press*, Boca Raton (2012)
DOI: 10.1201/b12939
92. H. Feldman (Ed): Atlas of Alzheimer's Disease. *Informa Healthcare*, New York (2007)
DOI: 10.3109/9781435626133
93. C. Hu, R. Ju, Y. Shen, P. Zhou, and Q. Li: Clinical decision support for Alzheimer's disease based on deep learning and brain network. In: 2016 IEEE International Conference on Communications (ICC), 1–6 (2016)
94. E. Challis, P. Hurley, L. Serra, M. Bozzali, S. Oliver, and M. Cercignani: Gaussian process classification of Alzheimer's disease and mild cognitive impairment from resting-state fMRI. *NeuroImage*112, 232–243 (2015)
DOI: 10.1016/j.neuroimage.2015.02.037
95. T. Exarchos, A. Papadopoulos, and D. Fotiadis (Eds): Handbook of Research on Advanced Techniques in Diagnostic Imaging and Biomedical Applications. *IGI Global*, (2009)
DOI: 10.4018/978-1-60566-314-2
96. "The diffusion tensor, and its relation to FA, MD, AD and RD," <http://www.diffusion-imaging.com/2015/10/what-is-diffusion-tensor.html>
97. W. Hecke, L. Emsell, and S. Sunaert (Eds): Diffusion Tensor Imaging. *Springer* (2015)
98. C. Wee, P. Yap, J. Brownnyke, G. Potter, D. Steffens, K. Welsh-Bohmer, L. Wang, and D. Shen: Accurate identification of MCI patients via enriched white-matter connectivity network. In: Machine Learning in Medical Imaging. MLMI 2010. Lecture Notes in Computer Science, 6357. Eds: F Wang, P Yan, K Suzuki, D Shen Springer, Berlin, Heidelberg, 140–147 (2010)
DOI: 10.1007/978-3-642-15948-0_18
99. E. Schwab, M. Yassa, M. Weiner, and R. Vidal: Using automatic HARDI feature selection, registration, and atlas building to characterize the neuroanatomy of A β pathology. In: Computational Diffusion MRI. Mathematics and Visualization. Eds: A Fuster, A Ghosh, E Kaden, Y Rathi, M Reisert Springer, Cham, 207–218 (2016)
100. R. Polikar, C. Tilley, B. Hillis, and C. Clark: Multimodal EEG, MRI and PET data fusion for Alzheimer's disease diagnosis. *Conf Proc IEEE Eng Med Biol Soc*2010, 6058–6061 (2010)
101. P. Kanel, Xiuwen Liu, and W. Mio: Early detection of Alzheimer's based on intrinsic measurements. In: 2011 IEEE International Conference on Bioinformatics and Biomedicine Workshops (BIBMW), IEEE, Atlanta, GA, 1014–1016 (2011)
DOI: 10.1109/BIBMW.2011.6112543
102. D. Zhang, and D. Shen: Multi-modal multi-task learning for joint prediction of multiple regression and classification variables in Alzheimer's disease. *NeuroImage*59, 895–907 (2012)
DOI: 10.1016/j.neuroimage.2011.09.069
103. D. Kim, S. Kim, S. Risacher, L. Shen, M. Ritchie, M. Weiner, A. Saykin, and K. Nho: A graph-based integration of multimodal brain imaging data for the detection of early mild cognitive impairment (E-MCI). *Multimodal Brain Image Anal*8159, 159–169 (2013)
104. H. Suk, and D. Shen: Deep learning-based feature representation for AD/MCI classification. *Med Image Comput Comput Assist Interv*16, 583–590 (2013)
DOI: 10.1007/978-3-642-40763-5_72
105. B. Jie, D. Zhang, B. Cheng and D. Shen: Manifold regularized multi-task feature selection for multi-modality classification in Alzheimer's disease. *Med Image Comput Comput Assist Interv*16, 275–283 (2013)
DOI: 10.1007/978-3-642-40811-3_35
106. H. Suk, S. Lee, and D. Shen: Hierarchical feature representation and multimodal fusion with deep learning for AD/MCI diagnosis. *NeuroImage* 101, 569–582 (2014)
DOI: 10.1016/j.neuroimage.2014.06.077
107. H. Suk, S. Lee, and D. Shen: Latent feature representation with stacked auto-encoder for AD/MCI diagnosis. *Brain Struct Funct*220, 841–859 (2013)
DOI: 10.1007/s00429-013-0687-3
108. R. Li, W. Zhang, H. Suk, L. Wang, J. Li, D. Shen, and S. Ji: Deep learning based imaging data completion for improved brain disease diagnosis. *Med Image Comput Comput Assist Interv*17, 305–312 (2017)

109. S. Liu, S. Liu, W. Cai, S. Pujol, R. Kikinis, and D. Feng: Early diagnosis of Alzheimer's disease with deep learning. In: 2014 IEEE 11th International Symposium on Biomedical Imaging (ISBI), IEEE, Beijing, China, 1015–1018 (2014)
110. S. Liu, S. Liu, W. Cai, H. Che, S. Pujol, R. Kikinis, D. Feng, M. Fulham and ADNI: Multimodal neuroimaging feature learning for multiclass diagnosis of Alzheimer's disease. *IEEE Trans Biomed Eng*62, 1132–1140 (2015)
DOI: 10.1109/TBME.2014.2372011
111. B. Shi, Y. Chen, P. Zhang, C. Smith and J. Liu: Nonlinear feature transformation and deep fusion for Alzheimer's Disease staging analysis. *Pattern Recogn* 66, 487–498 (2017)
DOI: 10.1016/j.patcog.2016.09.032
112. F. Li, L. Tran, K. Thung, S. Ji, D. Shen, and J. Li: A robust deep model for improved classification of AD/MCI patients. *IEEE J Biomed Health Inform*19, 1610–1616 (2015)
DOI: 10.1109/JBHI.2015.2429556
113. W. Zhang, H. Shen, Z. Ji, G. Meng, and B. Wang: Identification of Mild Cognitive Impairment Using Extreme Learning Machines Model. In: Intelligent Computing Theories and Methodologies, Lecture Notes in Computer Science, 9226. Eds: DS Huang, KH Jo, A Hussain Springer, Cham, 589–600 (2015)
114. B. Cheng, M. Liu, H. Suk, D. Shen, and D. Zhang: Multimodal manifold-regularized transfer learning for MCI conversion prediction. *Brain Imag Behav*9, 913–926 (2015)
DOI: 10.1007/s11682-015-9356-x
115. B. Cheng, M. Liu, and D. Zhang: Multimodal multi-label transfer learning for early diagnosis of Alzheimer's disease. In: Machine Learning in Medical Imaging. MICCAI 2015. Lecture Notes in Computer Science, 9352. Eds: L Zhou, L Wang, Q Wang, Y Shi Springer, Cham, 238–245 (2015)
116. M. Weiner, P. Aisen, C. Jack, W. Jagust, J. Trojanowski, L. Shaw, A. Saykin, J. Morris, N. Cairns, L. Beckett, A. Toga, R. Green, S. Walter, H. Soares, P. Snyder, E. Siemers, W. Potter, P. Cole, and M. Schmidt: The Alzheimer's disease neuroimaging initiative:

progress report and future plans. *Alzheimers Dement*6, 202–211e7 (2010)
DOI: 10.1016/j.jalz.2010.03.007

Abbreviations: AD: Alzheimer's disease; CNS: central nervous system; MCI: mild cognitive impairment; PNS: peripheral nervous system; MRI: magnetic resonance imaging; DTI: diffusion tensor imaging; WM: white matter; CAT: computer axial tomography; fMRI: functional magnetic resonance imaging; SPECT: single photon emission computed tomography; PET: positron emission tomography; ECT: emission-computed tomography; NC: normal control; aMCI: amnesic MCI; dMCI: dysexecutive MCI; PCA: principal component analysis; SOM: self-organizing map; HV: hippocampal volume; TBM: tensor-based morphometry; CTH: cortical thickness; MBL: manifold-based learning; SVM: support vector machine; LDA: linear discriminant analysis; CAD: computer-aided diagnosis; BFO: bacterial foraging optimization; ANN: artificial neural network; LBP: local binary pattern; LTP: local ternary pattern; DLBP: dominant local binary pattern; CLBP: complete local binary pattern; ALBP: adaptive local binary pattern; LQP: local quinary pattern; LGS: local graph structure; GM: gray matter; CNN: convolutional neural networks; 3D: 3 Dimensional; PLS: partial least squares; RBF: radial basis function; ICA: independent component analysis; MCI-C: MCI converters; MCI-NC: MCI non-converters; 3D CAE: 3D convolutional auto-encoder; ISML: inherent structure-based multiview learning; HKS: heat kernel signature; SIHKS: scale-invariant HKS; WKS: wave kernel signature; rCBF: regional cerebral blood flow; PiB: pittsburgh compound b; ¹⁸F-FDG: ¹⁸f-2fluoro-2-deoxy-d-glucose; FDR: fisher discriminant ratio; AR: association rule; AE: activation estimation; ROI: region of interest; NMF: nonnegative matrix-factorization; DMN: default mode network; GP: Gaussian process; KNN: k-nearest neighbors; EM: expectation-maximization; RF: random forest; SD: standard deviation; VAF: voxel-as-features; NMSE: normalized minimum square error; KPCA: kernel PCA; BOLD: blood oxygen level dependent; rsfMRI: resting state fMRI; axial diffusivity: ADT; radial diffusivity: RD; FA: fractional anisotropy; MD: mean diffusivity; DWI: diffusion-weighted images; Aβ: beta-amyloid; EEG: electroencephalogram; M3T: multi-modal multi-task; MTFS: multi-task feature selection; M2TFS: multi-task feature selection; SAE: stacked auto-encoders; SK: single-kernel, MK: multi-kernel; DM: deformation magnitudes; ELM: extreme learning machine; M2TL: multimodal manifold-regularized transfer learning; MMD: maximum mean discrepancy; MDML: multimodal multi-label transfer learning;

SCTIMST: Sree Chitra Tirunal institute for medical science and technology; OASIS: open access series of imaging studies; BoF: bag of features; NF: neighborhood filter; LB: Laplace-Beltrami; MTL: medial temporal lobe; ADNI: Alzheimer's disease neuroimaging association; CSF: cerebrospinal fluid; SIFT: scale-invariant feature transform; Tc-99m-HMPAO: technetium-99m-hexamethylpropylene amine oxime; Tc-99m-ECD: Tc-99m-ethyl cysteinatodimer; Tc-99m-MI-BI: Tc-99m-methoxyisobutylnitrile; FLT: (F-18)-fluoro-3'-deoxy-3'-l-fluorothymidine; GE: general electric; pAD: prodromal AD; DLFC: dorsolateral prefrontal cortex; EADC: European Alzheimer's disease consortium; DVR: distribution volume ratio; BLSA: Baltimore longitudinal study of aging; RT: repetition time; TE: echo time; MDEFT: modified driven equilibrium Fourier transform; EPI: echo planar; LDDMM: large deformation diffeomorphic metric mapping; HCP: hippocampal connectivity project; CIND: center for imaging of neurodegenerative diseases; UCSF: university of California San Francisco; HARDI: high angular resolution diffusion imaging; ERP: event related potential; SSL: semi-supervised learning; VBM: voxel based morphometry; E-MCI: Early MCI; NIFTI: neuroimaging informatics technology initiative; CMRGlc: cerebral metabolic rate of glucose consumption; TML: thin-plate splines (TPS) metric learning; DSAE: denoising sparse auto-encoder; GP-LR: Gaussian process logistic regression; AC-PC: anterior and posterior commissures;

Key Words: Alzheimer's disease, Early Diagnosis, Medical Imaging Modalities, Clinical Findings, Computer-Based Findings, Fusion, Review

Send correspondence to: Ayman El-Baz, Bioengineering Department, University of Louisville, Louisville, KY, USA, Tel: 502-852-5092, Fax: 502-852-1577, E-mail: aselba01@louisville.edu